WAPD-TM-1385
DOE RESEARCH AND
DEVELOPMENT REPORT



# SUMMARY OF THE THERMAL EVALUATION OF LWBR

(LWBR Development Program)

MARCH 1980

CONTRACT DE-AC11-76PN00014



BETTIS ATOMIC POWER LABORATORY
WEST MIFFLIN, PENNSYLVANIA

Operated for the U. S. Department of Energy by
WESTINGHOUSE ELECTRIC CORPORATION

## DISCLAIMER

WAPD-TM-1385

# SUMMARY OF THE THERMAL EVALUATION OF LWBR
(LWBR Development Program)

Written by:

S. Lerner, K.D. McWilliams, J.W. Stout and J.R. Turner

With Technical Contributions from:

P.R. Bengel, S. Lerner, P.S. Marinkovich,
K.D. McWilliams, H. Renner, P. Sherba,
L.I. Steiner, J.W. Stout, J.R. Turner

March 1980

Contract No. DE-AC11-76PN00014

Printed in the United States of America
Available from the
National Technical Information Service
U.S. Department of Commerce
5285 Port Royal Road
Springfield, Virginia 22151

NOTE

This document is an interim memorandum prepared primarily for internal reference and does not represent a final expression of the opinion of Westinghouse. When this memorandum is distributed externally, it is with the express understanding that Westinghouse makes no representation as to completeness, accuracy, or usability of information contained therein.

BETTIS ATOMIC POWER LABORATORY
WEST MIFFLIN, PENNSYLVANIA 15122

Operated for the U.S. Department of Energy by
WESTINGHOUSE ELECTRIC CORPORATION

# FOREWORD

The Shippingport Atomic Power Station located in Shippingport, Pennsylvania was the first large-scale, central-station nuclear power plant in the United States and the first plant of such size in the world operated solely to produce electric power. This program was started in 1953 to confirm the practical application of nuclear power for large-scale electric power generation. It has provided much of the technology being used for design and operation of the commercial, central-station nuclear power plants now in use.

Subsequent to development and successful operation of the Pressurized Water Reactor in the Atomic Energy Commission (now Department of Energy, DOE) owned reactor plant at the Shippingport Atomic Power Station, the Atomic Energy Commission in 1965 undertook a research and development program to design and build a Light Water Breeder Reactor core for operation in the Shippingport Station.

The objective of the Light Water Breeder Reactor (LWBR) program has been to develop a technology that would significantly improve the utilization of the nation's nuclear fuel resources employing the well-established water reactor technology. To achieve this objective, work has been directed toward analysis, design, component tests, and fabrication of a water-cooled, thorium oxide-uranium oxide fuel cycle breeder reactor for installation and operation at the Shippingport Station. The LWBR core started operation in the Shippingport Station in the Fall of 1977 and is expected to be operated for about 4 to 5 years or more. At the end of this period, the core will be removed and the spent fuel shipped to the Naval Reactors Expended Core Facility for a detailed examination to verify core performance including an evaluation of breeding characteristics.

In 1976, with fabrication of the Shippingport LWBR core nearing completion, the Energy Research and Development Administration, now DOE, established the Advanced Water Breeder Applications (AWBA) program to develop and disseminate technical information which would assist U.S. industry in evaluating the LWBR concept for commercial-scale applications. The program is exploring some of the problems that would be faced by industry in adapting technology confirmed in the LWBR program. Information being developed includes concepts for commercial-scale prebreeder cores which would produce uranium-233 for light water breeder cores while producing electric power, improvements for breeder cores based on the technology developed to fabricate and operate the Shippingport LWBR core, and other information and technology to aid in evaluating commercial-scale application of the LWBR concept.

All three development programs (Pressurized Water Reactor, Light Water Breeder Reactor, and Advanced Water Breeder Applications) are under the technical direction of the Office of the Deputy Assistant Secretary for Naval Reactors of DOE. They have the goal of developing practical improvements in the utilization of nuclear fuel resources for generation of electrical energy using water-cooled nuclear reactors.

Technical information developed under the Shippingport, LWBR, and AWBA programs has been and will continue to be published in technical memoranda, one of which is this present report.

INTENTIONALLY BLANK

TABLE OF CONTENTS


| | | Page |
|---|---|---|
| I. | INTRODUCTION | 1 |
| II. | BACKGROUND | 2 |
| | A. Core Mechanical Description | 2 |
| | B. Thermal-Hydraulic Description and Related Unique Features | 9 |
| | 1. Hydraulic Balancing of Movable Fuel | 17 |
| | 2. Module Inlet and Outlet Orificing | 17 |
| | 3. Axial and Radial Fuel Zoning | 20 |
| | 4. Small Rod-to-Rod Spacing | 20 |
| | 5. Hydraulic Coupling of Two Different Rod Diameter Regions | 22 |
| III. | BASIS FOR PERFORMANCE EVALUATION | 22 |
| | A. Critical Heat Flux | 23 |
| | B. Flow Stability | 23 |
| IV. | GENERAL ANALYTICAL PROCEDURE | 24 |
| | A. Pressure-Drop Forcing Function | 24 |
| | B. Maximum Resistance Thermal Model | 26 |
| | C. Hot Channel Allowances | 26 |
| | D. Thermal Capability | 27 |
| V. | ANALYTICAL MODELS FOR XITE AND HOTROD | 28 |
| | A. XITE Models | 28 |
| | B. HOTROD Models | 34 |
| | 1. Seed Model | 36 |
| | 2. Blanket Model | 38 |
| | 3. Blanket and Power-Flattening-Blanket Interface Model | 38 |
| | 4. Type IV Reflector Model | 38 |
| VI. | HOT CHANNEL ALLOWANCES | 42 |
| | A. Nuclear Allowances | 42 |
| | B. Engineering (Mechanical) Allowances | 42 |
| | 1. Heat Input Hot Channel Factors | 46 |
| | 2. Channel Flow Hot Channel Factors | 46 |
| VII. | SUMMARY OF THERMAL PERFORMANCE | 48 |
| | A. Critical Heat Flux Performance | 48 |
| | 1. Overpower Accident | 50 |
| | 2. Loss-of-Flow Accident | 53 |
| | B. Flow Stability Performance | 54 |

TABLE OF CONTENTS (Cont'd)


| | | Page |
|---|---|---|
| VIII. | QUALIFICATION | 55 |
| IX. | CONCLUSION | 58 |
| X. | REFERENCES | 60 |
| XI. | ACKNOWLEDGEMENT | 62 |
| APPENDIX A - ANALYTICAL CORRELATIONS | | A-1 |
| A. | Critical Heat Flux | A-1 |
| B. | Heat Transfer | A-2 |
| C. | Pressure Drop | A-5 |
| D. | References | A-6 |

## LIST OF TABLES


| Table | Title | Page |
|---|---|---|
| I | Core Parameters | 9 |
| II | Hydraulic Biases | 25 |
| III | A. Nuclear Uncertainty Factors | 43 |
| | B. Thermal Off-Equilibrium Factors | 45 |
| IV | Hot Channel Factors | 47 |
| V | Summary of the Minimum Power Ratios for LWBR Steady-State/Transient Conditions | 49 |
| VI | Electrically-Heated Rod Bundle CHF Test Geometry | 56 |
| VII | LWBR CHF and Pressure-Drop Correlation Parameter-Range Summary | 59 |


## LIST OF FIGURES


| Figure | Title | Page |
|---|---|---|
| 1 | Module Identification | 3 |
| 2 | Type I Module Cross Section | 5 |
| 3 | Type II Module Cross Section | 6 |
| 4 | Type III Module Cross Section | 7 |
| 5 | Type IV and Type V Reflector Module Cross Section | 8 |
| 6 | Type I Seed Region Radial Power Distribution at Beginning of Core Life | 11 |
| 7 | Type I Seed Region Axial Power Distribution at Beginning of Life for Rod Row 11 | 12 |
| 8 | Type I Blanket Rod Radial Power Distribution at Beginning of Core Life | 13 |
| 9 | Type I Blanket Region Axial Power Distribution at Beginning of Life for Rod Row 5 | 14 |
| 10 | LWBR Core in Shippingport Reactor Vessel Showing Core Hydraulic Flow Paths | 16 |
| 11 | Variable Geometry Nuclear Control Concept | 18 |

LIST OF FIGURES (cont'd)


| Figure | Title | Page |
|---|---|---|
| 12 | Blanket Module Assembly Showing Orifice Plates | 19 |
| 13 | Schematic of Type I Module Fuel Compositions | 21 |
| 14 | LWBR Seed XITE Analysis Model | 29 |
| 15 | LWBR Blanket XITE Analysis Model | 31 |
| 16 | LWBR Power-Flattening Blanket XITE Analysis Models | 32 |
| 17 | LWBR Reflector XITE Analysis Model | 33 |
| 18 | Location of HOTROD Thermal Analysis Blocks | 35 |
| 19 | LWBR Seed HOTROD Analysis Model | 37 |
| 20 | LWBR Blanket HOTROD Analysis Model | 39 |
| 21 | LWBR Blanket/Power-Flattening Blanket HOTROD Analysis Model | 40 |
| 22 | LWBR Reflector HOTROD Analysis Model | 41 |
| 23 | LWBR Thermal Capability Vs. Lifetime | 51 |
| 24 | LWBR CHF Power Capability (by Region) Vs. Lifetime | 52 |
| 25 | Comparison of Measured and Predicted Critical Heat Fluxes for LWBR Test Bundles at 2000 Psia | 57 |

This report describes the thermal evaluation of the core for the Shippingport Light Water Breeder Reactor. This core contains unique thermal-hydraulic features such as (1) close rod-to-rod proximity, (2) an open-lattice array of fuel rods with two different diameters and rod-to-rod spacings in the same flow region, (3) triplate orifices located at both the entrance and exit of fuel modules and (4) a hydraulically-balanced movable-fuel system coupled with (5) axial-and-radial fuel zoning for reactivity control. Performance studies used reactor thermal principles such as the hot-and-nominal channel concept and related nuclear/engineering design allowances. These were applied to models of three-dimensional rodded arrays comprising the core fuel regions. Digital computer programs were employed to assess the core capability using qualified procedures, models and correlations. The evaluation demonstrates that thermal-hydraulic design objectives and criteria are satisfied for operation of the core in the Shippingport Reactor Plant.

# SUMMARY OF THE THERMAL EVALUATION OF LWBR (LWBR Development Program)

S. Lerner, K.D. McWilliams, J.W. Stout, J.R. Turner

## I. INTRODUCTION

The Light Water Breeder Reactor (LWBR) Program is developing the technology to breed fissile material in a light water reactor in order to use nuclear fuel more efficiently in light water thermal reactors. This core represents the first full-core power reactor usage of a thoria-base binary fuel of high density.

This report describes the thermal evaluation of the LWBR core. The hydraulic evaluation of the LWBR design is presented in Reference (1) and an overall view of the design is presented in Reference (2). The LWBR core design includes several unique thermal-hydraulic features. These features are described in Section II and result from the overall objective to demonstrate breeding in a light water environment. Sections III through VI provide a description of the analytical procedures and models developed to

assess the core thermal capability. A summary of the core thermal performance is given in Section VII and the experimental qualification of the procedures is presented in Section VIII.

## II. BACKGROUND

### A. Core Mechanical Description

The design of LWBR was controlled to a large extent by the breeding objective. This objective necessitated minimizing parasitic neutron losses within the constraints permitted by mechanical and thermal requirements. In general, this meant that the number and size of mechanical structures were minimized and that the fuel rods were spaced as closely together as practical.

Figure 1 shows a cross section of the LWBR core installed in the Shippingport pressurized-water reactor vessel. The core is a seed-blanket configuration consisting of an inner region of movable-fuel seed assemblies, each surrounded by a stationary blanket assembly. Zircaloy structural shells separate each seed and blanket assembly. The combination of one seed and one blanket assembly constitutes a module. The inner region has twelve hexagonal modules (Types I, II and III) arranged in a symmetric array. These modules are surrounded by an outer reflector fuel region composed of fifteen modules (Types IV and V). The core design was developed for operation with the existing major components of the Shippingport Plant, including the pumps, piping systems, heat exchangers and 109-inch inside-diameter reactor vessel. The design simulates a large-scale breeder environment in the interior of the core (three Type I modules) with the intent to achieve net breeding in the entire core.

The core has four distinct fuel regions -- seed, blanket, power-flattening blanket and the reflector. The first three of these are arranged within the inner twelve modules. The Type I module is a symmetrical hexagon in which the standard blanket region forms an annular hexagonal ring about the seed region. The Type II and Type III modules are symmetric non-regular

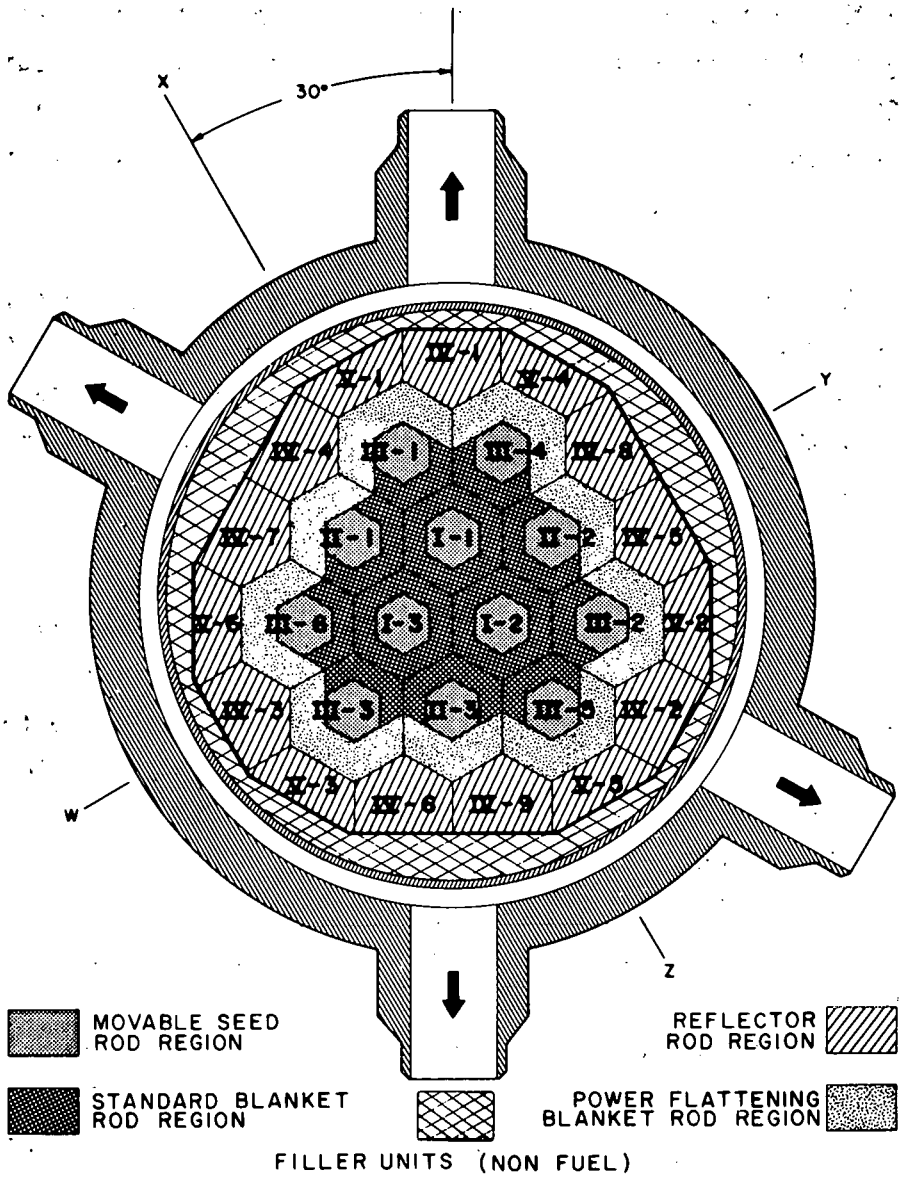


FIGURE I. MODULE IDENTIFICATION

hexagons with the elongated, larger cross sections containing the power-flattening blanket fuel rods. The seed and these two blanket regions contain about 14,200 Zircaloy-clad fuel rods having fissile fuel (U-233) in the form of thoria-urania ($ThO_2$-$UO_2$) fuel pellets and fertile material in the form of thoria ($ThO_2$) fuel pellets.

The reflector modules serve to restrict neutron loss from the core and contain about 3000 Zircaloy-clad fuel rods bearing only $ThO_2$ fuel pellets. Similarly, thoria fuel in the seed and blanket is located at the top and bottom of these regions to act as an axial reflector. Filler modules, which are solid blocks of steel, surround the core to minimize bypass flow between the active core and the LWBR core barrel.

To enhance breeding performance, the standard blanket region has a high metal-to-water ratio of 2.98. The power-flattening-blanket region has a lower metal-to-water ratio of about 1.76 and a higher $UO_2$ concentration than the blanket. The power-flattening blanket is located on the outer periphery of the nine modules surrounding the three center modules. As a result, the overall radial core power distribution is flattened.

The rods in all fuel regions are approximately 10 feet long and are supported in a closely-spaced, triangular-pitched array by stainless-steel, honeycomb support grids at several axial locations within each module. The grid support system is described in Reference (3). There are nine axial levels of grids for the seed, eight for each blanket and six for the reflector fuel rods. Figures 2, 3, 4 and 5 show details, such as the rod diameter and pitch, of the five module types in the core cross section.

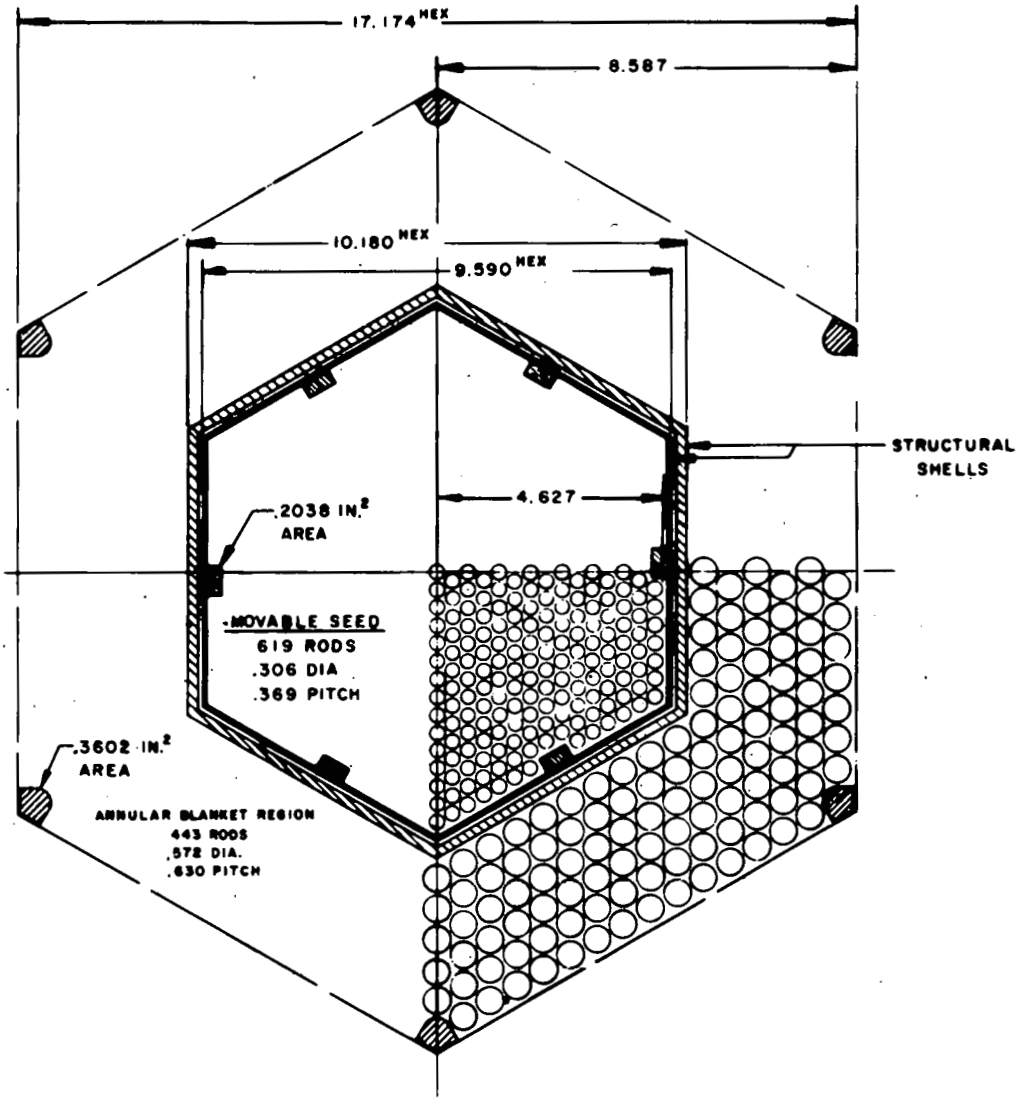


FIGURE 2. TYPE I MODULE CROSS SECTION

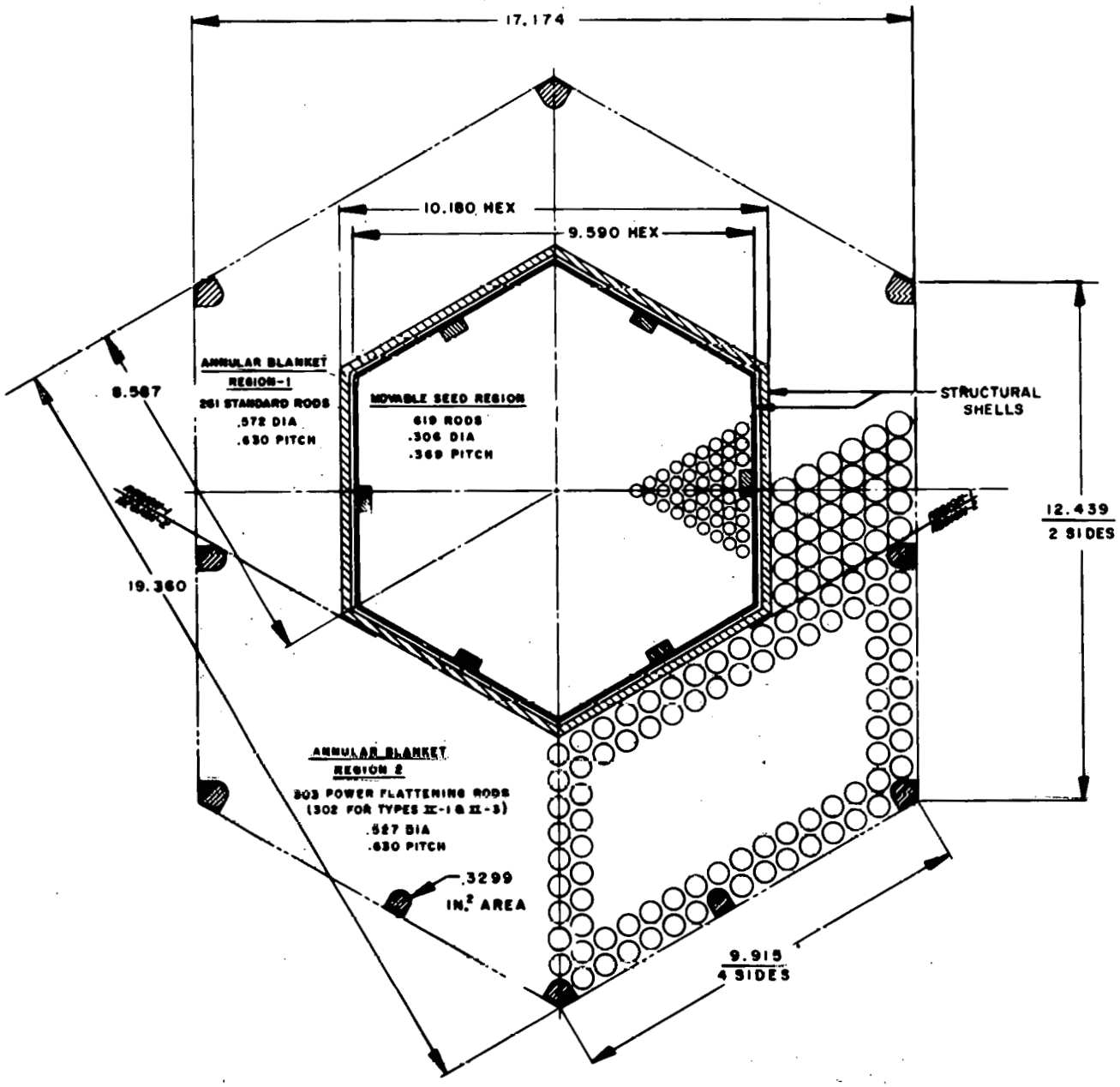


FIGURE 3. TYPE II MODULE CROSS SECTION

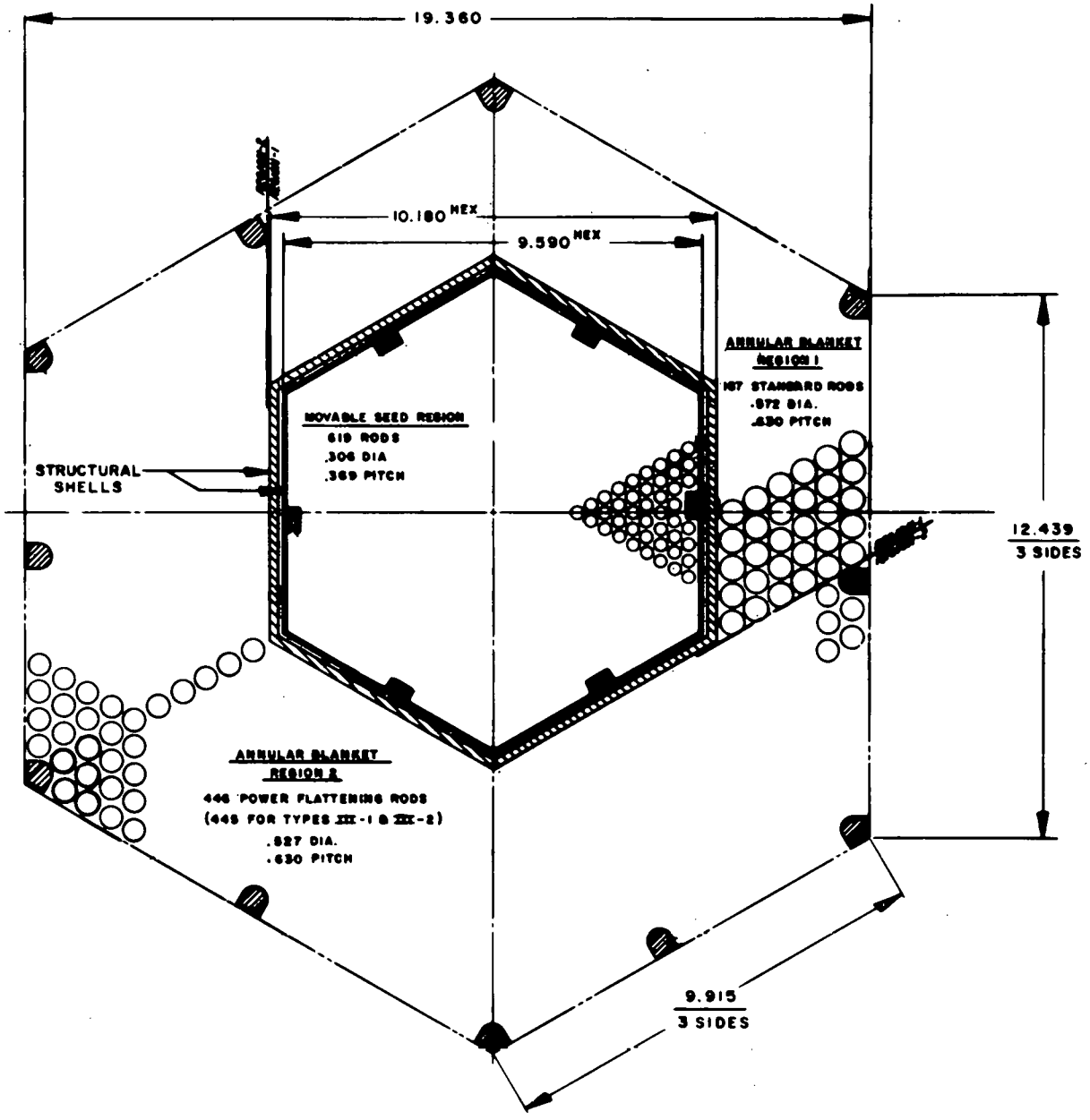


FIGURE 4. TYPE III MODULE CROSS SECTION

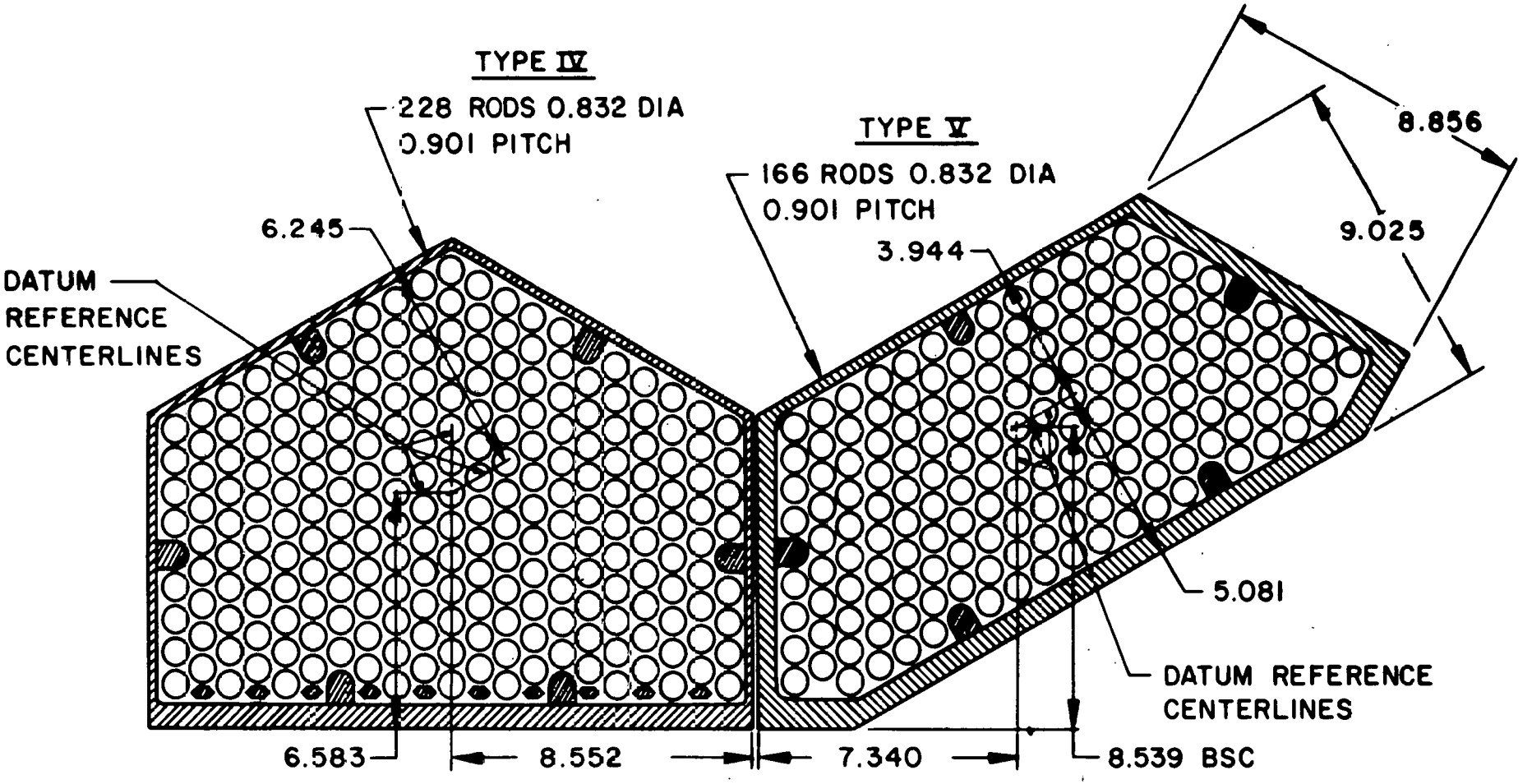


FIGURE 5. TYPE IV AND TYPE V REFLECTOR MODULE CROSS SECTION

## B. Thermal-Hydraulic Description and Related Unique Features

The LWBR thermal performance was evaluated at a rated power of 236.6 thermal megawatts (equivalent to 72 gross electrical megawatts) and a total reactor coolant flow of about 31 x $10^6$ pounds per hour at an average temperature of 531°F (inlet temperature of 520°F) and operating pressure of 2000 psia. The different metal-to-water ratios and fissile fuel loadings required in each core region produced variations in the region average power densities. Table I shows core parameters and typical distribution of power and flow in the core by fuel region. Figures 6, 7, 8 and 9 show typical axial and radial power shapes for the Type I seed and blanket modules. Reference (4) provides more details about the nuclear design.

TABLE I

CORE PARAMETERS

| | Seed | Blanket | Power-Flattening Blanket | Reflector |
|---|---|---|---|---|
| Power Fraction | 0.380 | 0.321 | 0.298 | 0.001 |
| Flow* Fraction | 0.249 | 0.185 | 0.321 | 0.094 |
| Average Heat Flux @ 100% Power x $10^{-3}$, BTU/hr-ft$^2$** | 59.5 | 61.5 | 60.2 | 4.2 |
| Maximum Heat Flux @ 100% Power x $10^{-3}$, BTU/hr-ft$^2$** | 375. | 267. | 285. | 77. |
| Mass Velocity x $10^{-6}$, lb/hr-ft$^2$ | 2.409 | 2.225 | 2.696 | 0.737 |
| Fuel Rod Diameter, in. | 0.306 | 0.572 | 0.527 | 0.832 |
| Hydraulic Diameter (infinite array), in. | 0.187 | 0.198 | 0.309 | 0.246 |

TABLE I (cont'd)

| | Seed | Blanket | Power-Flattening Blanket | Reflector |
|---|---|---|---|---|
| Pitch, in. | 0.369 | 0.630 | 0.630 | 0.901 |
| Total Number | 7428 | 3234 | 3581 | 3047 |
| Number of Grid Levels | 9 | 8 | 8 | 6 |
| Flow Area, $ft^2$ | 2.839 | 2.545 | 3.698 | 4.103 |
| Heat Transfer Area, $ft^2$ | 5184. | 4220. | 4307. | 5667. |
| Heated Wetted Perimeter, in. | 7141. | 5803. | 5923. | 7964. |
| Unheated Wetted Perimeter, in. | 438. | 369. | 558. | 1049. |

* Remaining flow goes to movable fuel balancing system and bypass paths.

** Heat Fluxes are for 100 full power hours of operation except for the reflector which is at 18,000 hours. The heat flux in the reflector initially containing only thoria is low at beginning of life. With increasing lifetime, the thorium is transmuted to uranium-233 and the power generated in the reflector fuel rods increases.

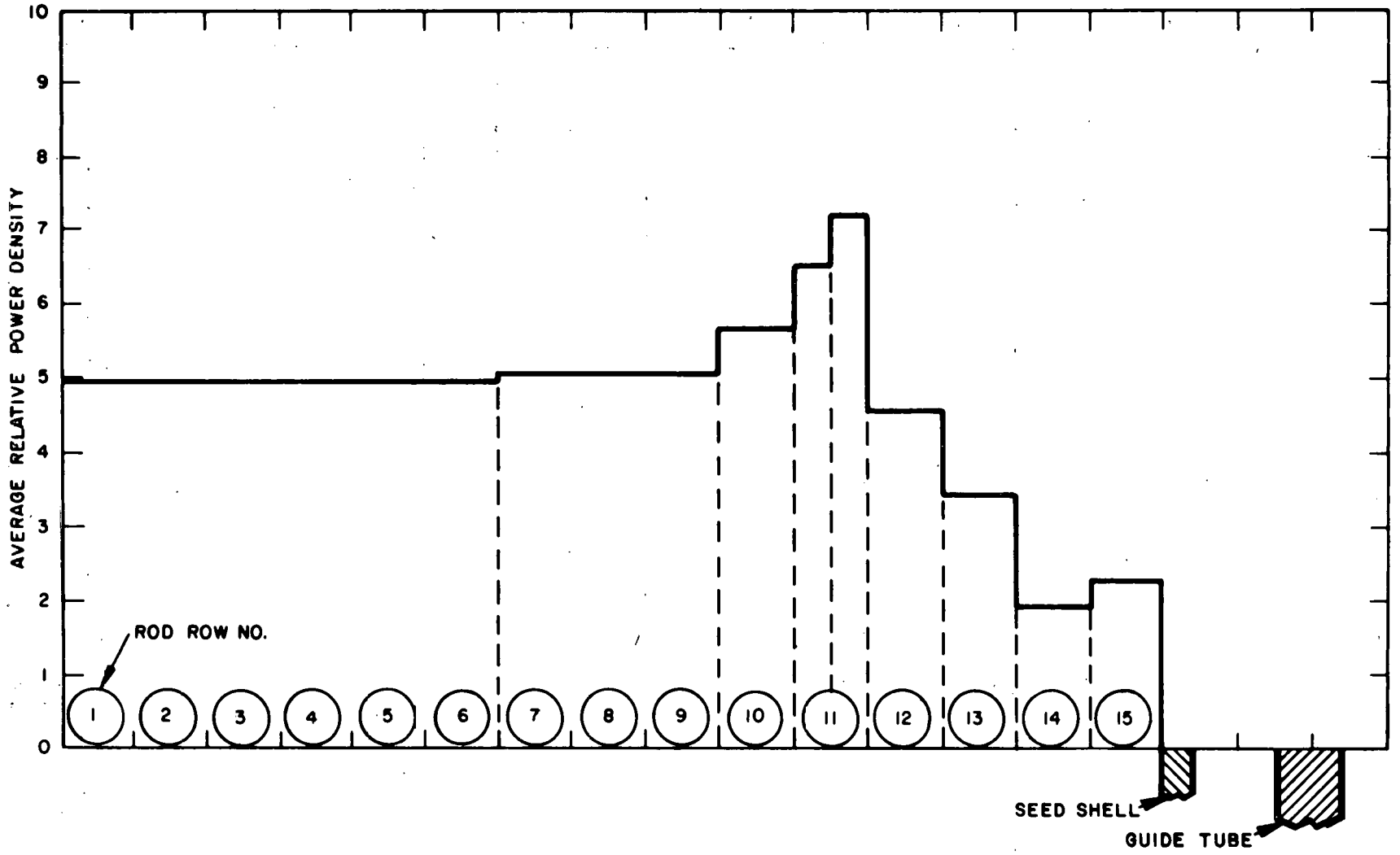


FIGURE 6. TYPE I SEED REGION RADIAL POWER DISTRIBUTION AT BEGINNING OF CORE LIFE

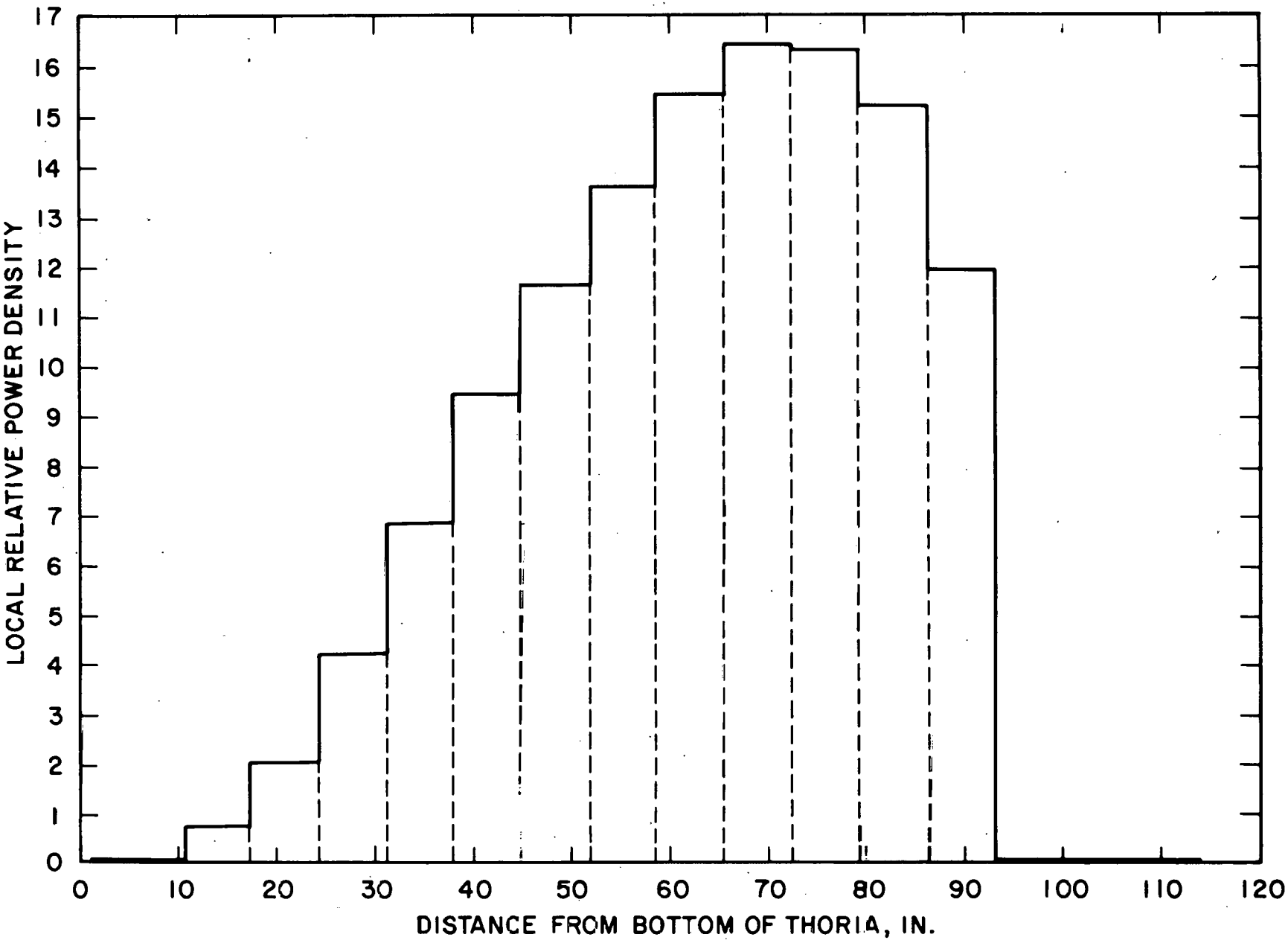


FIGURE 7. TYPE I SEED REGION AXIAL POWER DISTRIBUTION AT BEGINNING OF LIFE FOR ROD ROW 11

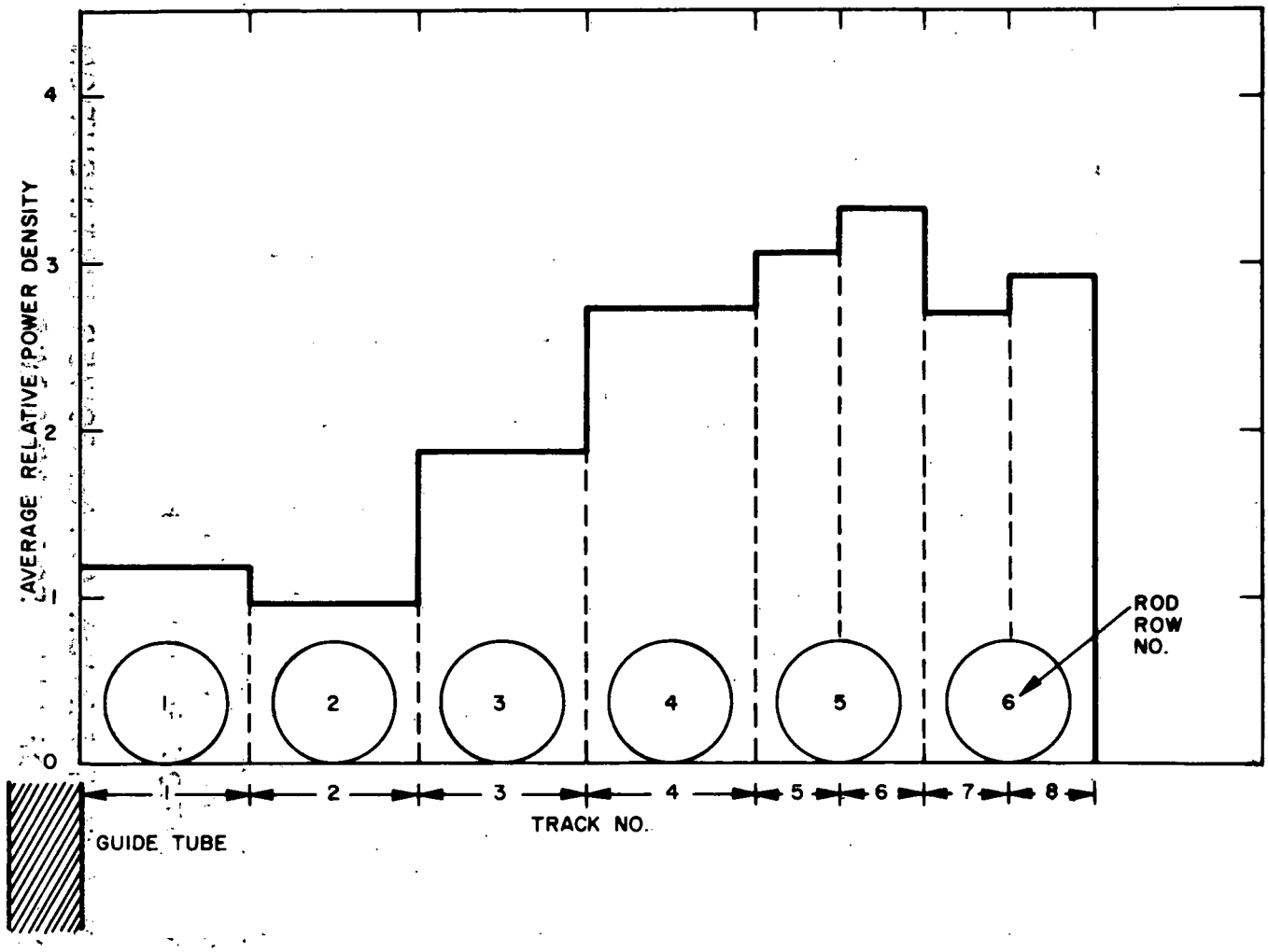


FIGURE 8. LWBR BLANKET ROD RADIAL POWER DISTRIBUTION AT BEGINNING-OF-CORE LIFE

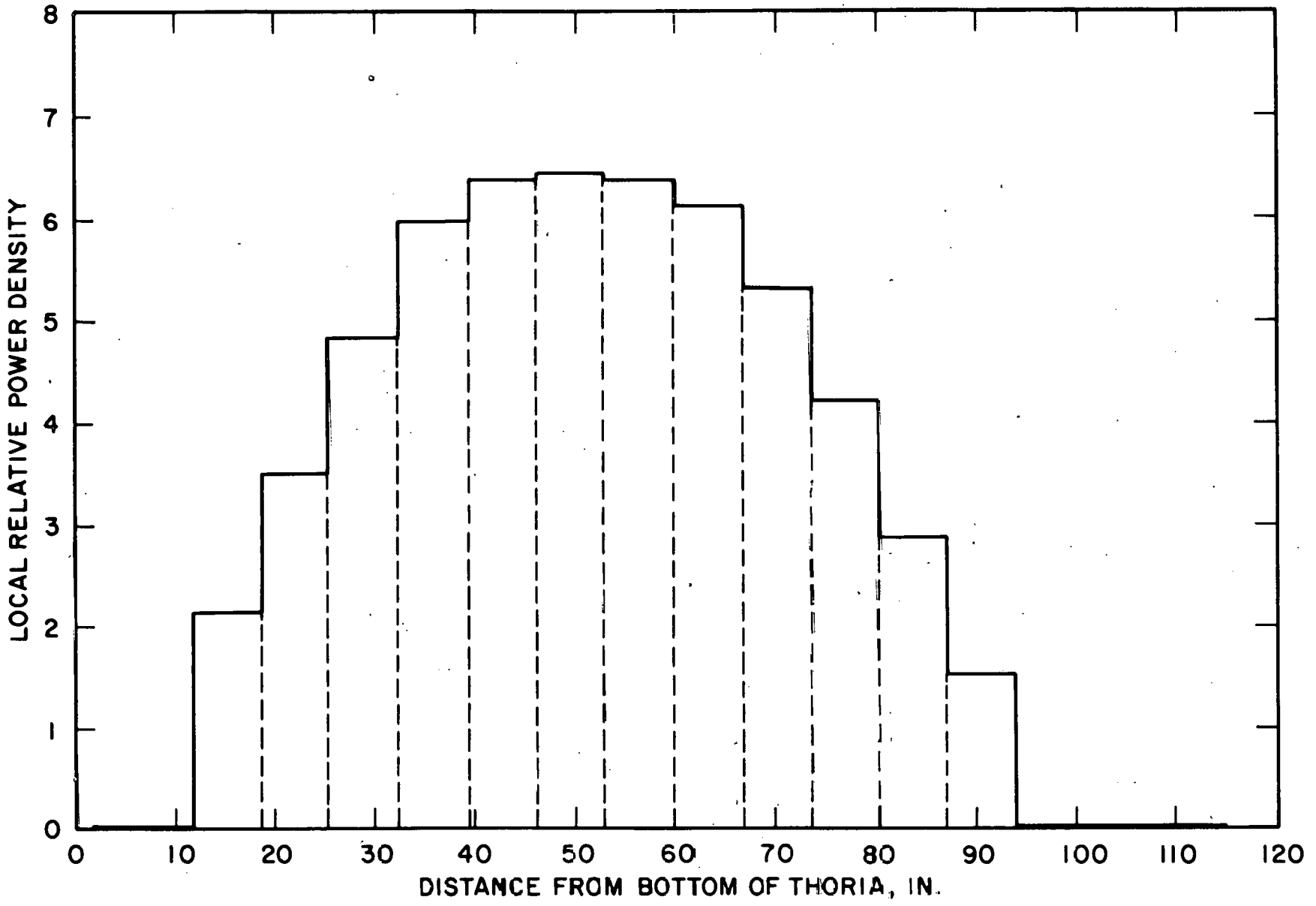


FIGURE 9. TYPE I BLANKET REGION AXIAL POWER DISTRIBUTION AT BEGINNING OF LIFE FOR ROD ROW 5

Figure 10 shows a schematic of the various flow paths through the one-pass core. Flow enters the reactor vessel through four bottom inlet nozzles. A portion of the inlet flow passes between the reactor vessel and the outer thermal shield to cool both the reactor vessel and thermal shield. This flow then rejoins the main coolant stream above the reactor inlet flow baffle where it proceeds into the four primary core regions, with the flow being proportioned as shown in Table I. The reactor inlet flow baffle is the same one used for Shippingport PWR Core 2 and acts as a flow straightener for the reactor vessel inlet plenum. In the core, coolant velocities are 16 ft/sec. (seed), 15 ft/sec. (blanket), 18 ft/sec. (power flattening blanket) and 4 ft/sec. (reflector). In the outlet plenum above the core, the flow from the various paths rejoins and emerges through the four reactor vessel outlet nozzles. Reference (1) provides a more detailed hydraulic description of the core.

During the development of the LWBR design, several unique features arose relating to the breeding and power objectives. These were associated with such concepts as: (a) movable-fuel reactivity control with hydraulic balancing,* (b) module inlet-and-outlet orificing with thin boundary shells to optimize the core flow distribution and pressure differences across the shells, (c) extensive fuel zoning incorporating a stepped fissile/fertile fuel arrangement with both an axial-and-radial fertile reflector, (d) rod-to-rod spacings about one-half that presently employed in pressurized-water reactors and (e) hydraulic coupling of fuel regions containing rods of different diameters on the same pitch. These features received extensive thermal-and-hydraulic testing and performance evaluation during the development phase to provide a high degree of design assurance for core operation. Additional facets of the design, testing and qualification are highlighted below.

---

* Bypass Inlet Flow (BIF) System

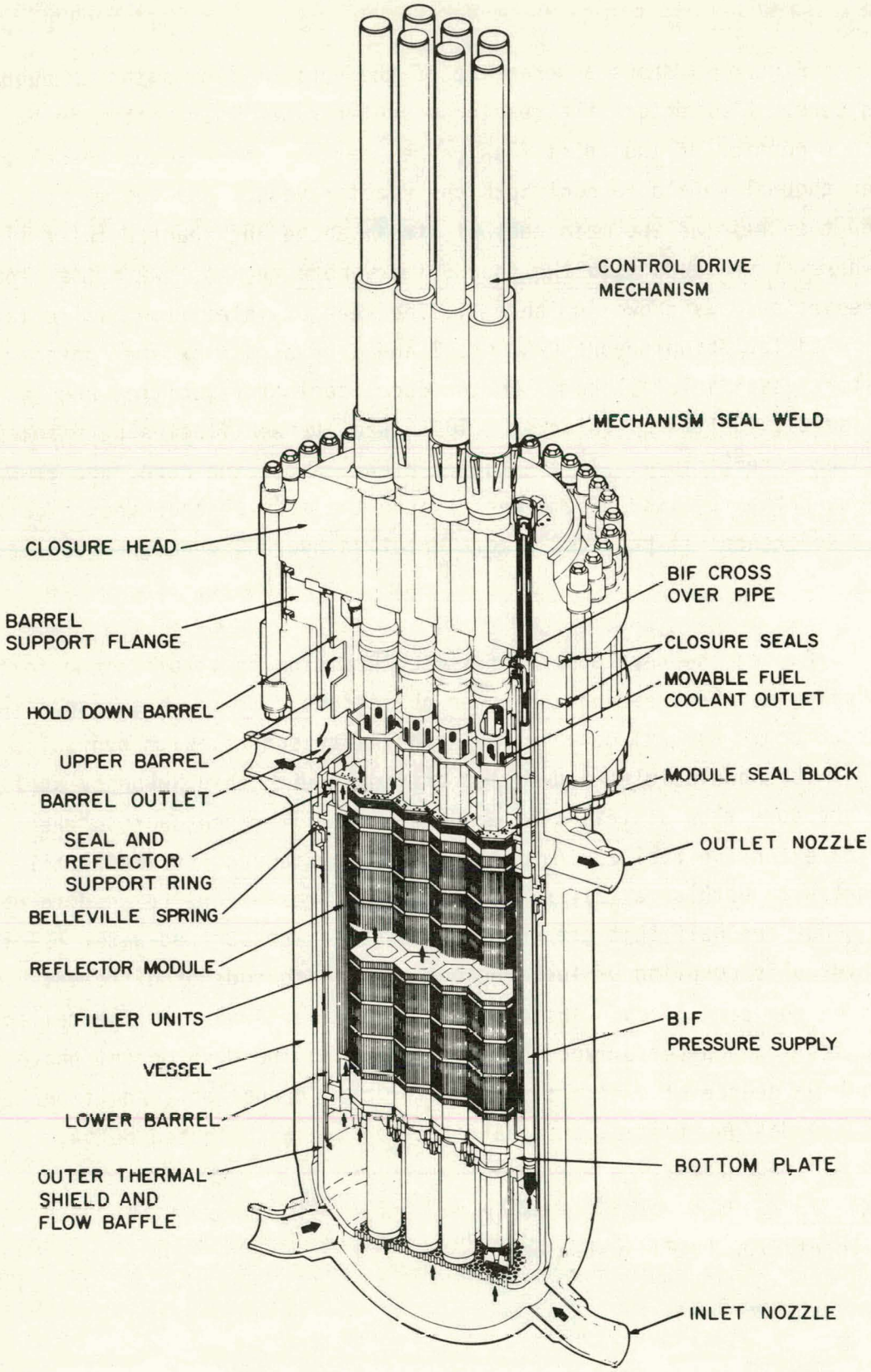


FIGURE 10. LWBR CORE IN SHIPPINGPORT REACTOR VESSEL SHOWING CORE HYDRAULIC FLOW PATHS

### 1. Hydraulic Balancing of Movable Fuel

Core reactivity is controlled by axial motion of the twelve movable fuel assemblies. These assemblies are maintained in a uniformly banked configuration during power operations. Each assembly is suspended from a control drive mechanism providing a seven-foot axial travel. The lower and upper limits of this travel consist of five feet below to two feet above the aligned configuration. Figure 11 shows the fuel configuration for both the aligned and full-down (or shutdown) positions. Power operations occur between about two feet below to two feet above the aligned position. This unique hydraulic feature, including its performance characteristics and full-scale testing (with successful operation at Shippingport), is described in greater detail in References (5), (6) and (7).

### 2. Module Inlet and Outlet Orificing

The use of seed, blanket, and reflector fuel regions with different fuel loadings and metal-to-water ratios causes significant power differences among the regions. To optimize flow utilization and core power capability, the blanket and reflector modules are orificed. The structural shells isolate the fuel regions to eliminate the potential for flow redistribution. Triplate orifices are utilized at both the top and bottom of the blanket and reflector modules, as illustrated in Figure 12, to reduce lateral loads on the shells by approximately 50 percent as compared with loads associated with only inlet orificing. The reduced load distribution minimizes the potential for shell deflection and increases assurance of a free path for scram of the movable fuel assemblies.

Testing of a full-size prototypic assembly of a section of the core confirmed the triplate orifice pressure-loss coefficients and the shell pressure loads, Reference (1). In addition, flows through seven of the seed modules and six of the blanket modules are measured at Shippingport. All data obtained during early operation demonstrated that flows are within the allowable range, confirming the acceptability of the orificing, Reference (7).

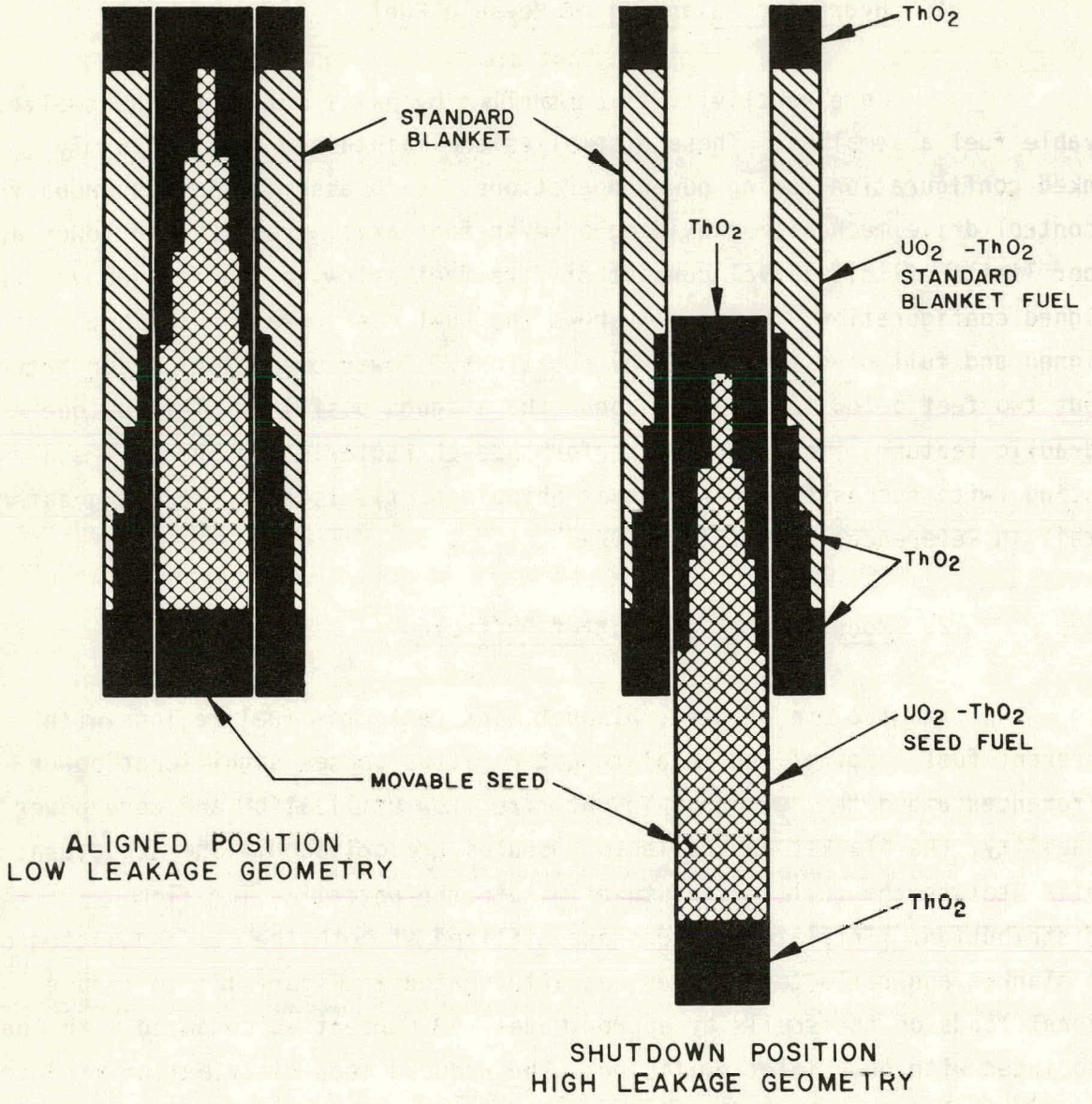


FIGURE II. VARIABLE GEOMETRY NUCLEAR CONTROL CONCEPT

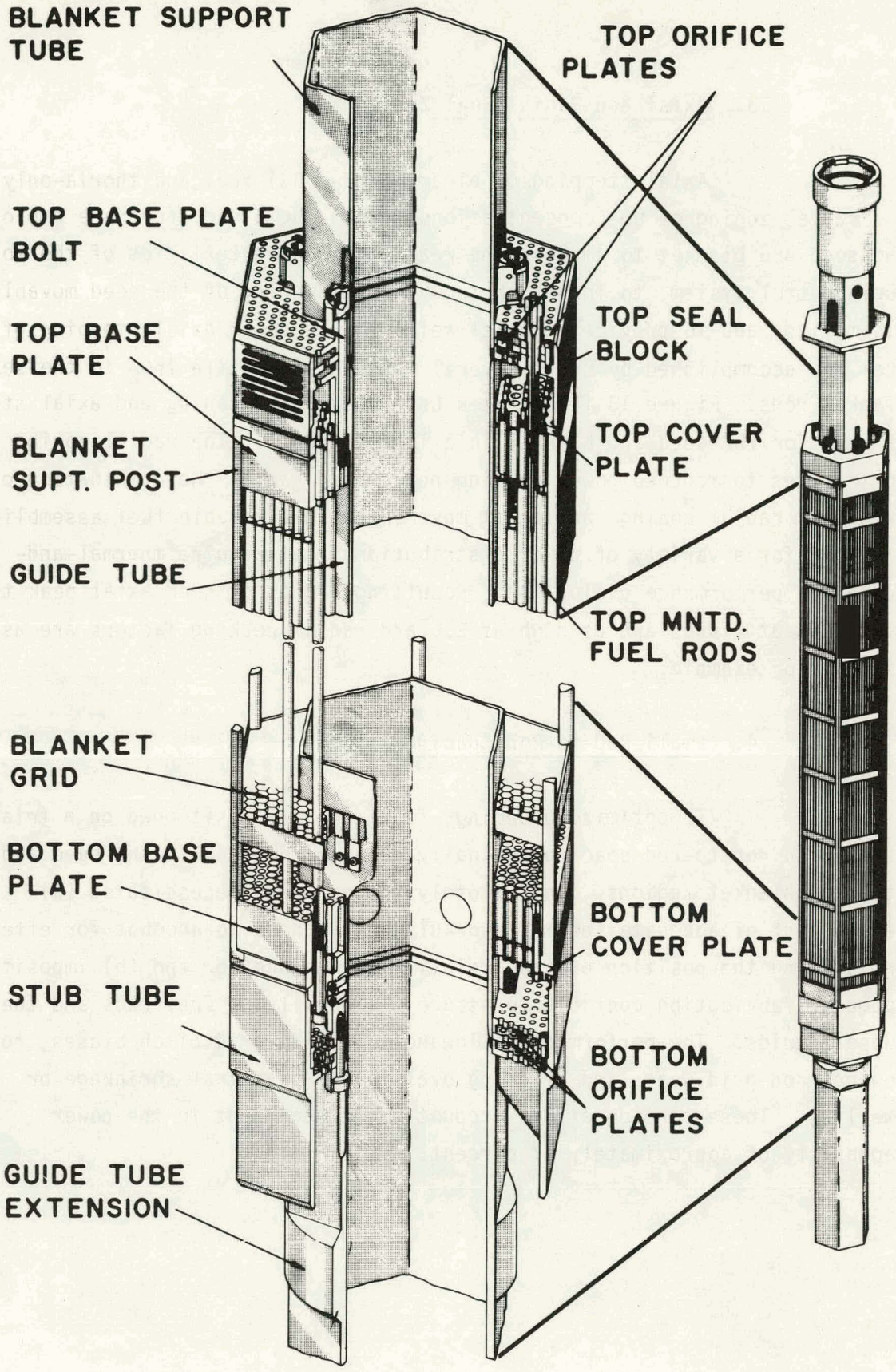


FIGURE 12. TYPE I BLANKET ASSEMBLY

### 3. Axial and Radial Fuel Zoning

Axial stepping of binary ($ThO_2$-$UO_2$) fuel and thoria-only fuel and radial zoning of $UO_2$ concentrations within the binary fuel are employed in the seed and blanket to improve the reactivity characteristics of the movable-fuel control system, to insure shutdown upon lowering of the seed movable-fuel assemblies, and to provide an axial reflector region. Axial stepping of the fuel was accomplished by using several lengths of fertile $ThO_2$ in the seed and blanket rods. Figure 13 illustrates both the radial zoning and axial stepping of fuel for the seed and blanket in a Type I module. The radial zoning contributes to reduced power peaking near water gaps. The combination of fuel stepping, radial zoning, and axial movement of the movable fuel assemblies accounts for a variety of power distributions that require thermal-and-hydraulic performance evaluation. Resulting ratios of seed axial peak-to-average heat fluxes are as high as 2.6 and radial peaking factors are as high as 2.4, for example.

### 4. Small Rod-to-Rod Spacing

To optimize breeding, fuel rods are positioned on a triangular pitch with rod-to-rod spacing nominally about 0.060 inch in the seed and standard blanket regions. This closely spaced array necessitated (a) development of adequate thermal/hydraulic allowances to account for effects influencing the position of rods relative to one another and (b) imposition of adequate fabrication controls to assure the quality of fuel rods and their support grids. The performance allowances include grid pitch biases, rod bowing, rod-grid wear, and cladding ovality and diametral shrinkage or swelling. These considerations account for a decrement in the power capability of approximately 17 percent.

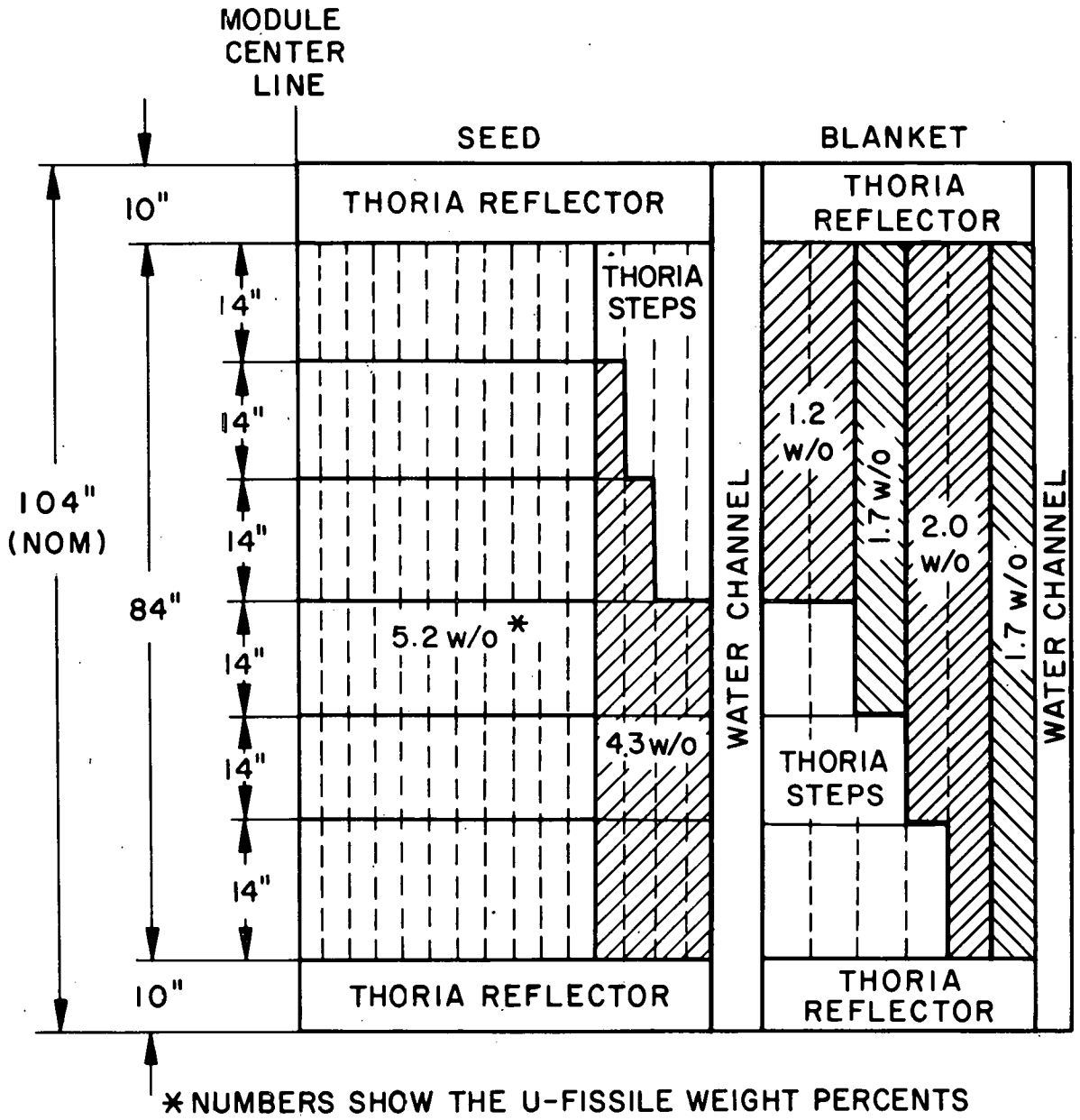


FIGURE 13. SCHEMATIC OF TYPE I MODULE FUEL COMPOSITIONS

### 5. Hydraulic Coupling of Two Different Rod Diameter Regions

As noted, the power-flattening blanket region was designed to have a lower metal-to-water ratio than the blanket region. Since the rods in these two regions are arranged with the same pitch, the diameters of the power-flattening blanket rods were made smaller than those in the standard blanket. The power-flattening blanket with about a 0.100-inch rod-to-rod spacing and a 1.2 pitch-to-diameter ratio is hydraulically coupled in an open lattice to the standard blanket with a 0.060-inch rod-to-rod spacing and pitch-to-diameter ratio of 1.1. Since the two adjacent blanket regions have different hydraulic resistances, different coolant velocities occur across their interface (18 ft/sec. versus 15 ft/sec). The inlet and outlet orifices are designed to apportion the flow to each blanket region so as to minimize cross flow. Hydraulic tests, including a prototypic test with the two coupled-blanket regions, verified that acceptable flow conditions existed between these two regions.

## III. BASIS FOR PERFORMANCE EVALUATION

The core thermal-and-hydraulic objective was to provide adequate fuel-rod heat transfer for normal reactor operation and postulated accident conditions. The core design provides coolant conditions to meet this objective and other fuel-rod performance requirements as given in Reference (2). The hydraulic aspects of the design, Reference (1), ensure reasonable fluid velocities for cooling and pressure distributions consistent with acceptable structural loads. Results obtained from analysis and test programs described later in this report and from prior PWR Core 1/PWR Core 2 design and operating experience, References (8) and (9), show the core is conservatively designed for operation at rated power.

The design has been evaluated for steady-state operation, plant operational transients, and postulated accident conditions resulting from operator or equipment faults, using the Design Power Ratio (DPR) concept* and two thermal criteria:

---

* The DPR is a numerical indication of the core power margin and is defined as the power to attain a thermal limit divided by the reactor power rating. For loss-of-flow accidents, the reactor power rating is taken as the maximum core power for the mode of operation just before the accident. For overpower accidents, the power rating is taken as the maximum core power that could result, including allowance for all protection system uncertainties, for the mode of operation.

A. Critical Heat Flux

A critical heat flux (CHF) condition shall not occur on any fuel rod in the core. The minimum DPR for the CHF shall be no less than 1.05.*

Critical heat flux represents a condition at which a small increase in heat flux could result in a relatively large increase in the fuel rod temperature. The CHF condition is discussed at length in standard texts, References (10) and (11). The functional relationship of CHF with respect to the parameters of importance (heat flux, coolant flow, enthalpy, pressure and geometry) has been determined experimentally (see Section VIII). By preventing CHF, adequate heat transfer is ensured between the fuel rod cladding and reactor coolant.

B. Flow Stability

The core fuel region gross and local flow shall be upward and stable with limited local cross-flow permissible. The minimum flow stability DPR shall be no less than 1.05.

The flow stability limit represents a condition at which a small increase in power could result in an unstable flow condition. This limit is imposed to insure that the core coolant shall not exhibit either sustained or transient flow oscillations, flow reversals, or intermittent unstable flow conditions during steady-state core operation, normal plant transients, or postulated accident conditions. Experimental tests have shown that open-matrix rod bundles such as those contained in LWBR are inherently conducive to flow stability as shown in Reference (12).

---

* The DPR for a CHF limit should not be confused with the standard critical heat flux ratio which is the ratio of the critical heat flux at the limiting core location to the local heat flux at a constant mass velocity in the hot channel. The critical heat flux ratio can give a falsely high indication of the power margin. The DPR is a truer measure of core power margin than is the critical heat flux ratio, because it accounts for the change in mass velocity in the hot channel as power is changed.

Reactor plant controls and setpoints, together with the blanket and reflector flow orificing, have been established to assure adequate performance with respect to the above two criteria.

## IV. GENERAL ANALYTICAL PROCEDURE

The objective of the thermal and hydraulic analysis is to determine a conservative set of local fluid conditions which define the allowable power to meet the criteria previously described. The analysis technique consists of four basic steps.

### A. Pressure-Drop Forcing Function

Thermal-analysis computer programs (Section IV-D) determine local fluid conditions in the hot channel for a given input pressure drop and power distribution. A lower-bound pressure drop along the fuel rod is defined using the procedures and models described in Reference (1). Briefly, this pressure drop is established by means of a hydraulic model of the entire primary side of the plant using the HAFMAT computer program. This program determines the core flow distribution and component pressure drops given the pump-head characteristics and the hydraulic resistances of all the loop and core components. To establish the pump head and component hydraulic resistance, nominal values are defined and then uncertainty bands are assigned to account for tolerances. The HAFMAT analysis is performed by applying the uncertainty limits in the direction of minimizing the pressure drop along a nominal fuel rod channel. Table II summarizes the direction in which the limits for pump head and hydraulic resistance are assumed (i.e., minimum or maximum).

TABLE II

HYDRAULIC BIASES

| Item | Bias | | | Comment |
|---|---|---|---|---|
| Pump-Head Curve | min* | | | Gives least available pump head |
| Loop Loss Coefficient | max* | | | Max.parasitic hydraulic losses to provide min. flow to rodded region |
| Reactor Inlet and Outlet Loss Coefficient | max | | | |
| Baffle Loss Coefficient and Thermal Shield | max | | | |
| | Seed | Blkt. | Refl. | |
| Flow Meter Loss Coefficient | max | max | -- | |
| Orifice Loss Coefficient | -- | max | max | |
| Base Plate Loss Coeff. | max | max | max | |
| Rod and Grid Loss Coefficient | min | min | min | Gives min. in-core pressure drop |
| Seed Annulus Loss Coefficient | | min | | Maximizes bypass flow in parallel with rodded region |
| Leakage Loss Coefficient (Core) | | min | | |
| BIF Loss Coefficient | | min | | |

* "min" is minimum.
"max" is maximum.

A fuel-region and time-dependent crud deposition model, Reference (13), is also used to produce a core lifetime-dependent pressure-drop forcing function for each of the four primary fuel regions of the core. This pressure-drop forcing function is adjusted to account for the possibility of flow maldistribution resulting from inlet and outlet plenum effects and preferential crud as discussed in Section VI.

B. Maximum Resistance Thermal Model

To account for the possibility that one local portion of a core fuel region could have a maximum hydraulic resistance (i.e., a hot channel), and therefore reduced flows, thermal models for each region of the core are established assuming that all resistances for fuel rods and grids are at the maximum side of their uncertainty bands. This maximum resistance model, along with the minimum pressure-drop forcing function, ensures that a conservative hydraulic environment is established.

C. Hot Channel Allowances

Thermal analytical models (described in Section V) assume nominal rod-to-rod spacing over the entire length of the fuel rods. The actual spacing varies because of grid dimensional tolerances and potential fuel rod effects such as bowing and cladding diametral-shrinkage, grooving, ovality and wear. To account for these effects, power penalties for the hot channels are defined. Similarly, mechanical effects producing potential heat flow asymmetry affecting enthalpy rise and local heat flux peaking are considered. These effects include pellets stacked off center, cladding ovality, and formation of inter-pellet axial gaps along the fuel pellet stack. The hot channel allowances are detailed in Section VI.

## D. Thermal Capability

The above three steps and the core power distribution are used with both two- and three-dimensional digital-computer programs to determine the thermal capability of the core. These programs are XITE, Reference (14), and HOTROD, Reference (15). In the analysis procedure, the enthalpy rise in the hot channel is calculated by using a subchannel model of the fuel regions which describes thermally limiting rods in detail (see Section V). Besides the limits applied to reactor plant controls, allowances are included for such items as manufacturing tolerances, crud, and uncertainties in the analytical or empirical descriptions used for nuclear, thermal, and hydraulic phenomena which occur in the core.

Overpower accidents are evaluated by the steady-state HOTROD program at a reference coolant temperature and pressure and an initial power level. The initial power is adjusted by the program to find the level at which CHF just occurs for the pressure drop imposed on the hot channel. HOTROD is also used to evaluate steady-state bulk boiling. Loss-of-flow accidents are analyzed using both the HOTROD and transient XITE programs with transient decay functions calculated by the XITE (Reference (14)), PARK (Reference (16)), and FIGRO (References (17), (18) and (19)) computer programs. The XITE program is also used to evaluate flow stability.

The XITE program treats two-dimensional conservation of mass, momentum and energy, along with the CHF and pressure-drop correlations described in Appendix A. The time derivative of fluid density is included in the continuity equations so that rapid transients can be analyzed. For transients, the time variation in power, inlet enthalpy, pressure, and either mass velocity or channel pressure drop are imposed as transient driving functions.

The HOTROD program is similar in concept to the three-dimensional COBRA-II program (Reference (20)), with improvements made in the numerical techniques and correlations. Like XITE, the HOTROD program permits a small amount of coolant mixing caused by the transverse redistribution of flow among

the subchannels to satisfy an axial momentum balance. In addition, a mixing model (Reference (21)) is incorporated into HOTROD to describe the turbulent-eddy-diffusion mixing of adjacent coolant streams in both the single- and two-phase coolant states of the fluid. This mixing effect reduces transverse enthalpy gradients caused by the nonuniform transverse power distribution in the rod array, and so HOTROD realistically predicts a higher, but still conservative, power capability compared to XITE. The HOTROD modeling otherwise incorporates the same correlations and parameters as does XITE.

A summary of the core thermal capability for limiting accidents, as determined by the above analysis procedure, is presented in Section VII.

## V. ANALYTICAL MODELS FOR XITE AND HOTROD

### A. XITE Models

The XITE seed model used to evaluate CHF, shown in Figure 14, simulates the equilateral triangular array of 619 rods including the annular channel formed by the seed shell (which contains one-inch-diameter holes to minimize transverse pressure differentials) and the stationary blanket guide tube. The model is composed of 10 tracks each depicting an annular hexagonal portion of the module rod array. Each track is described by an appropriate heated perimeter, wetted perimeter and flow area associated with the total number of rods within and the boundary characteristics of the given track cross section. With this representation, each rod of a given track is assigned the highest power input of any rod associated with that specific track. The azimuthal power is thus considered uniform and maximized. Each track is axially divided into thirty control-volume increments.

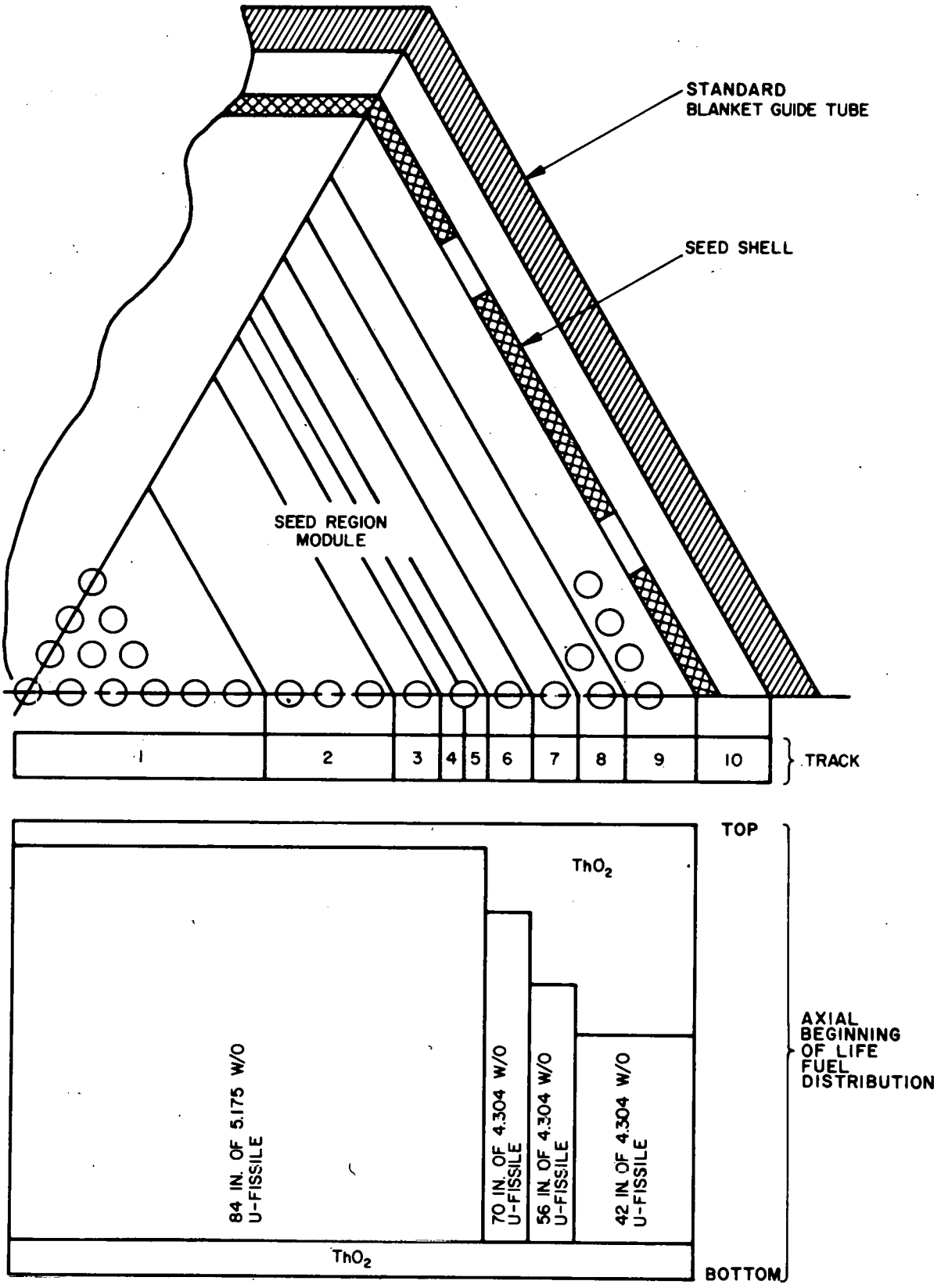


FIGURE 14. LWBR SEED XITE ANALYSIS MODEL

In Figure 14, Tracks 1, 2 and 3 depict several physical rows of rods in the inner part of the seed region where the radial power is uniform. Tracks 4 and 5 represent thermally limiting rods in Row 11, which is subdivided into an inner half (Track 4) and an outer half (Track 5). Rod Row 11 is divided in this way to account for the explicit power gradient which exists in this rod row as a result of its location adjacent to rod rows (Nos. 12 through 15 corresponding respectively to Tracks 6 through 9) of different fuel composition and fuel stack length. Track 10 represents an unheated annulus bounded by the seed shell and the blanket guide tube.

Two methods for hydraulic representation of the grids have been studied. These include (1) an explicit representation of the grid hydraulic loss coefficient within the control volume corresponding to the axial location of the grid, and (2) a distribution of the total grid loss coefficient in proportion to the axial length of each control volume (total of 30). The latter method resulted in the most conservative (lowest) prediction of allowable core power and is the one used for evaluation.

Similar thermal models were constructed for the standard blanket, power-flattening blanket, and reflector as shown in Figures 15, 16 and 17. As in the seed model, thermally limiting rod rows were subdivided into tracks to allow for the explicit representation of the radial power gradient. Posts used for grid support were conservatively depicted as power-producing rods. The method of grid simulation used for the seed was also applied to the blanket and reflector models.

For flow stability calculations, the XITE model depicts a single rod at the hottest power in the fuel region. A 5-percent pulse of 0.1-second duration is applied to the hot-channel pressure drop and the resultant flows are examined for stable performance (i.e., damped response).

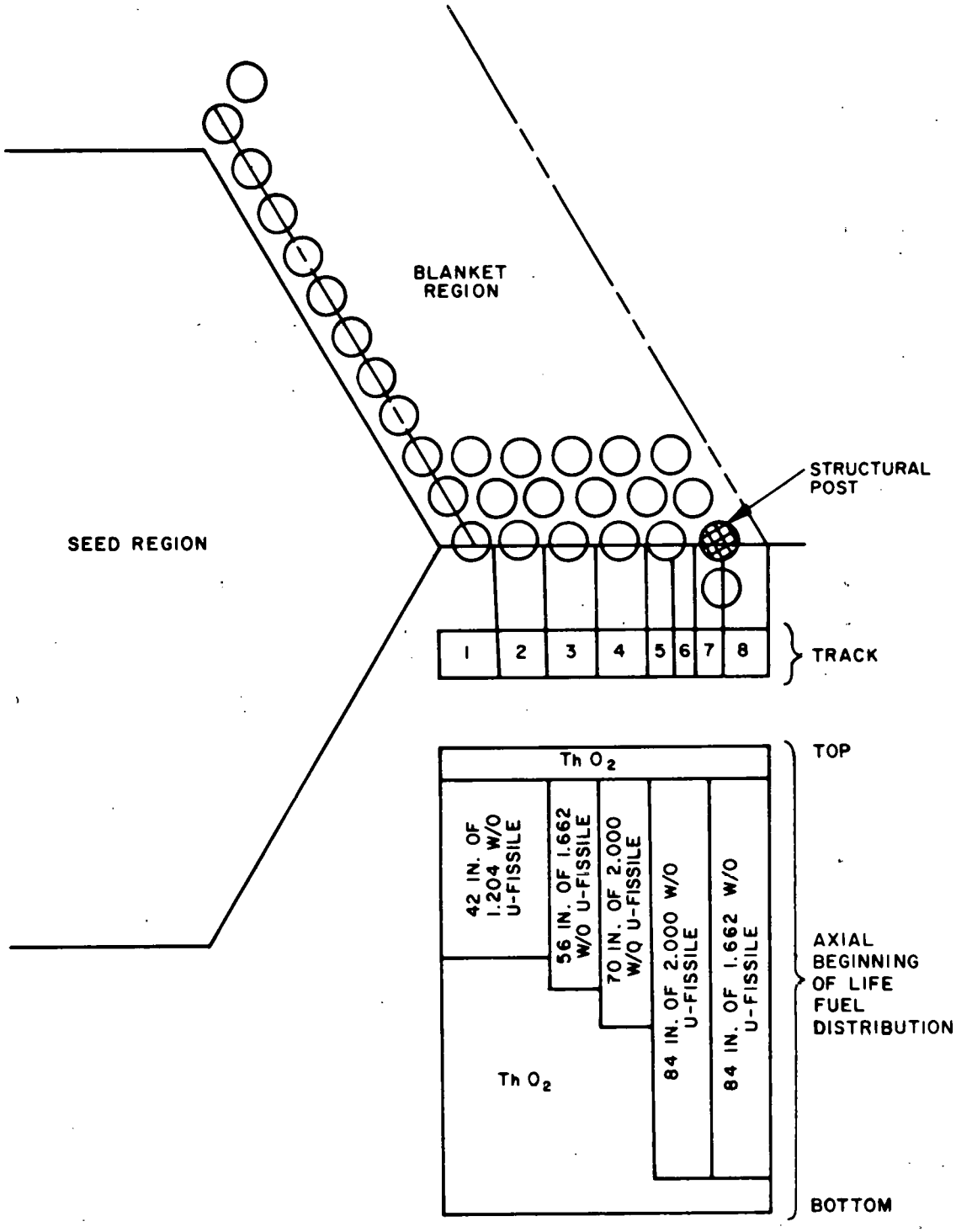


FIGURE 15. LWBR BLANKET XITE ANALYSIS MODEL

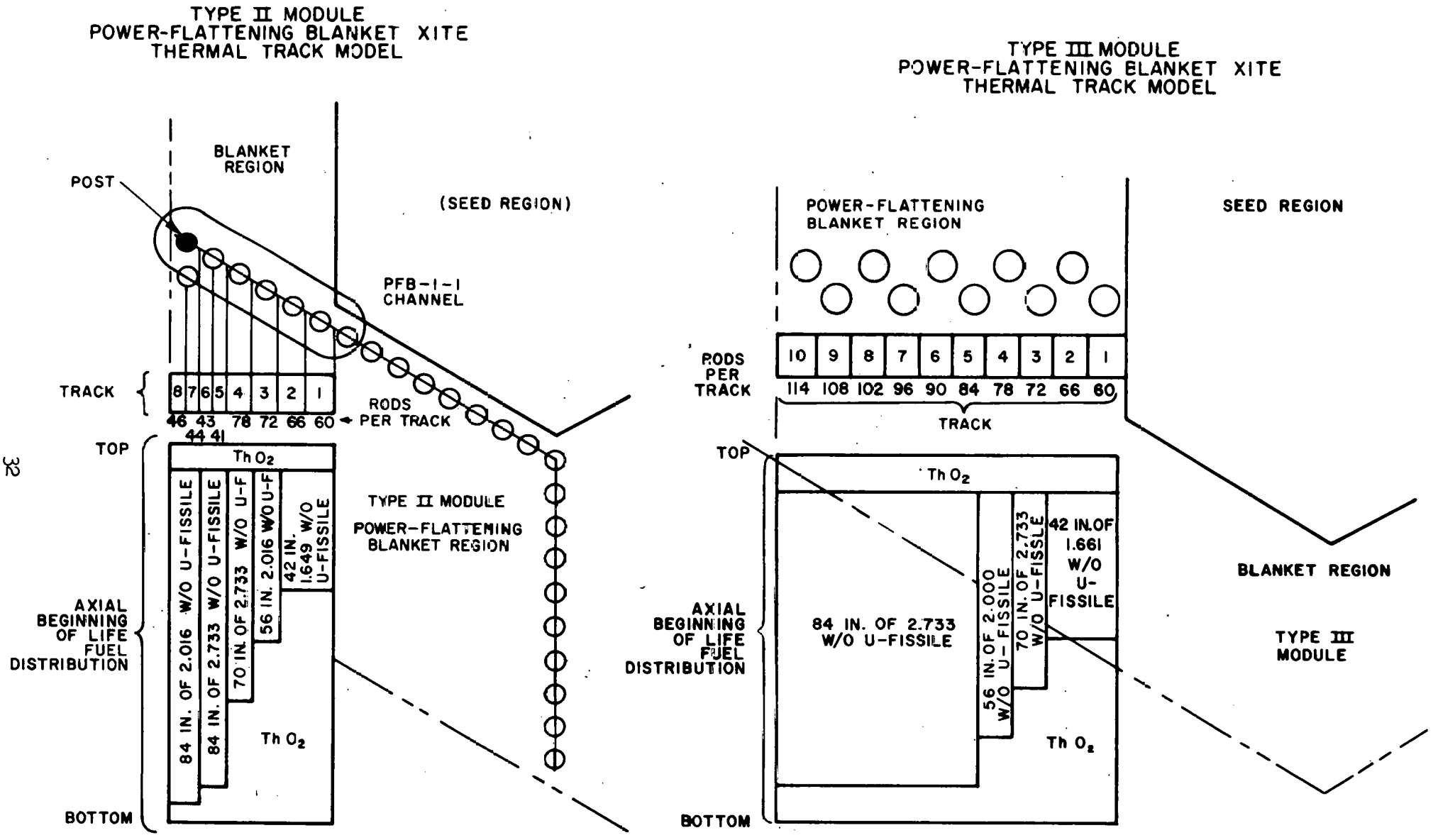


FIGURE 16. LWBR POWER-FLATTENING BLANKET XITE ANALYSIS MODELS

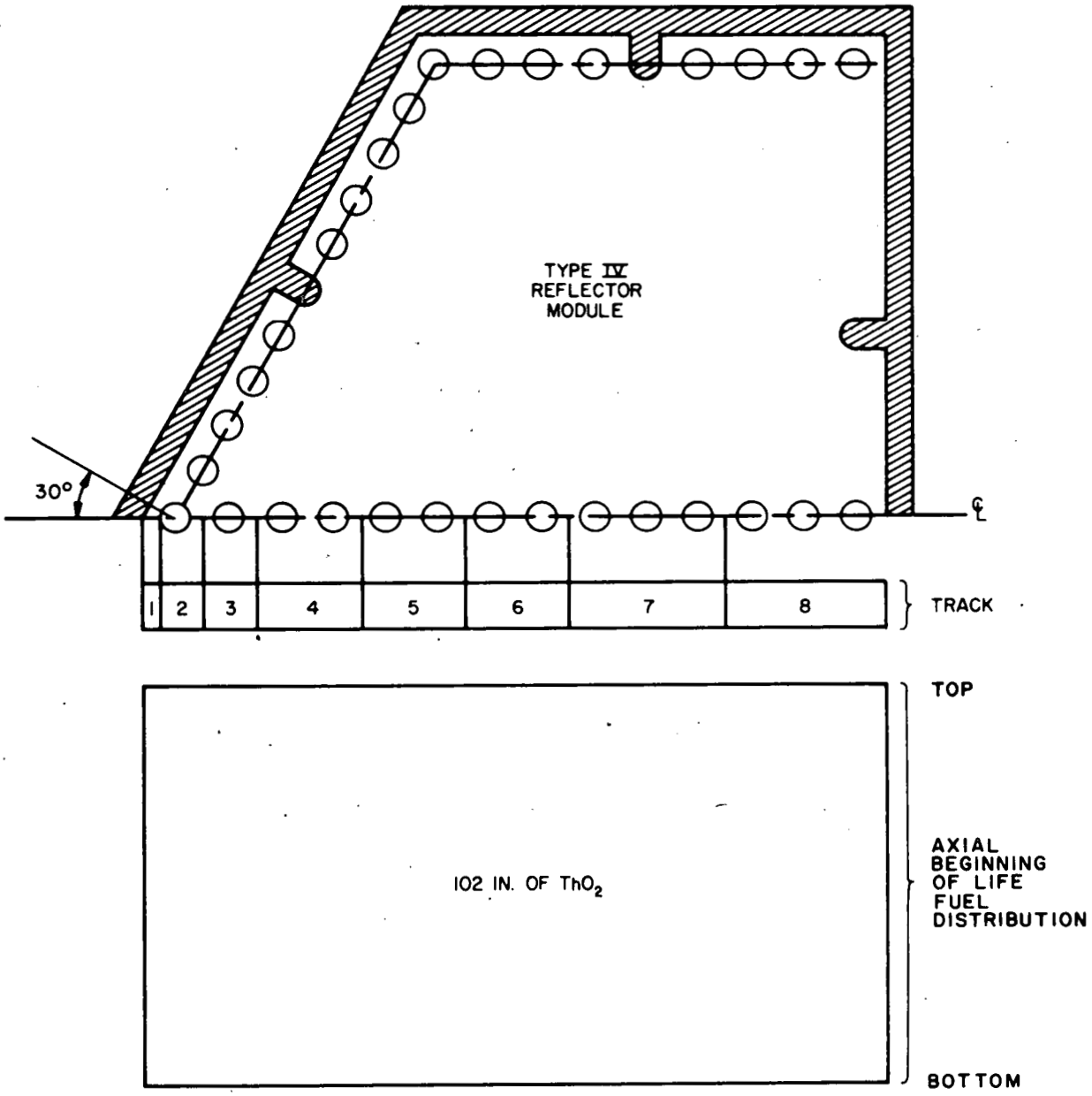


FIGURE 17. LWBR REFLECTOR XITE ANALYSIS MODEL

B. HOTROD Models

Three-dimensional HOTROD models present a more exact thermal-hydraulic representation of the flow area surrounding the fuel rods than do the XITE two-dimensional hot-channel track models. The HOTROD models were applied to a total of 38 thermal analysis blocks, shown in Figure 18, which mapped the power distribution within the one-sixth symmetrical core.

The fuel-rod and flow areas in the HOTROD subchannels are described by a hexagonal track arrangement whereby the subchannels enclose the fuel rods. In this subchannel arrangement, the hottest subchannels have greater detail than the cooler subchannels (through using half-hexagonal subchannels similar to the XITE half-track concept). The subchannels enclosing the hottest rods are surrounded by a buffer zone of adjacent subchannels. These buffer subchannels provide a transition zone away from the hottest subchannels by permitting a gradual increase in the size of the control volumes to include more fuel rods within a subchannel. The buffer model ensures that the thermal limit is reached first in the subchannels enclosing the hotter rods, since the benefits of transverse mixing are reduced by the buffer subchannels. This model predicts lower power levels to reach thermal limits compared to a model of lesser subchannel detail.

The hexagonal subchannels are used in the LWBR evaluation instead of an alternate triangular subchannel arrangement for determination of core thermal performance because:

(1) The hexagonal subchannels provide a means of keeping rods with dissimilar heat fluxes in different subchannels, thus predicting the inception of nucleate boiling at lower power levels.

(2) The hexagonal subchannel(s), each enclosing the rod(s), tend to increase the enthalpy rise for such rod(s). A comparison of the hexagonal and triangular subchannel concepts showed the hexagonal model to be conservative.

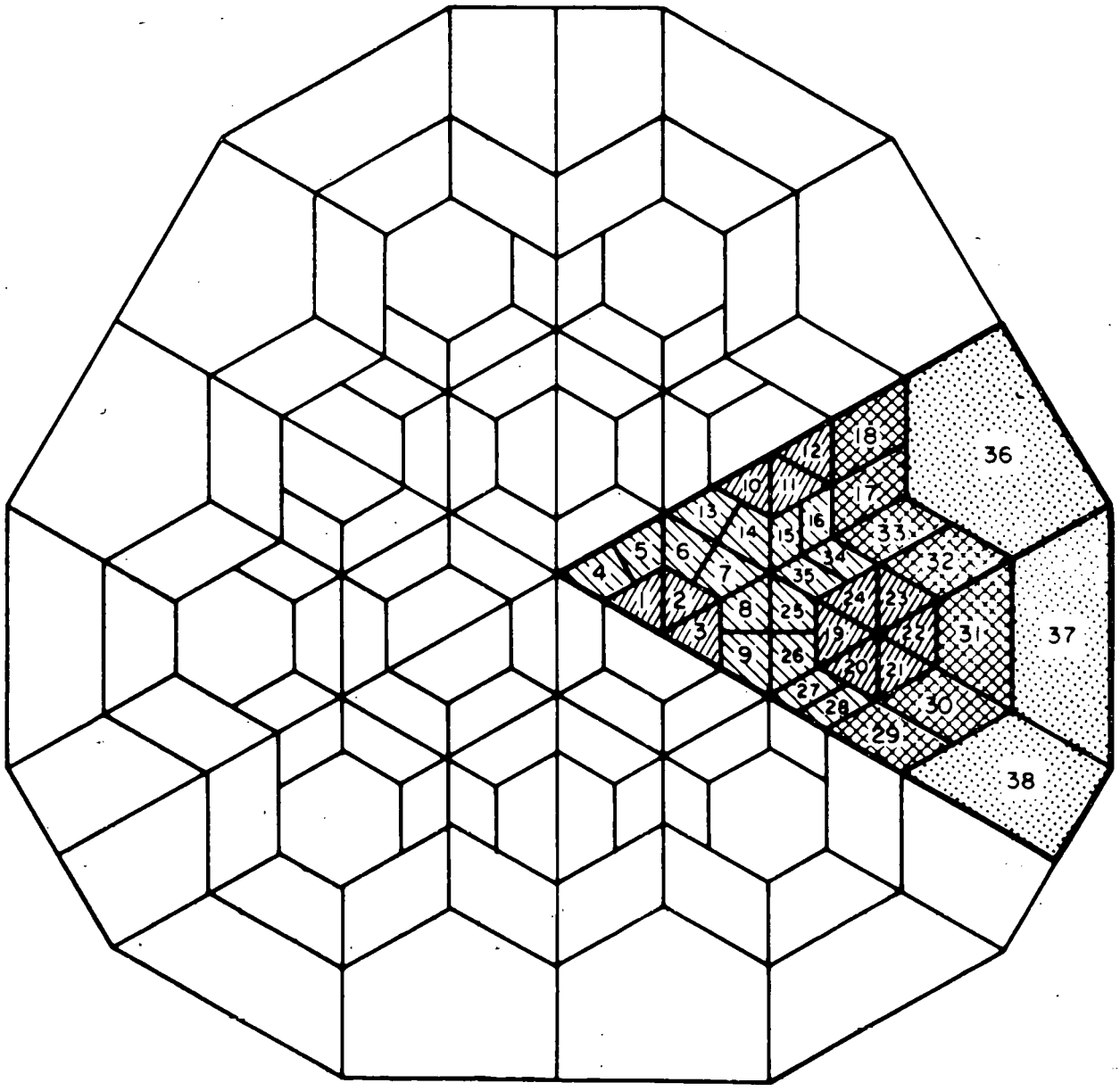


FIGURE 18. LOCATION OF HOTROD THERMAL ANALYSIS BLOCKS (LWBR 1/6-CORE SYMMETRY)

(3) The hexagonal subchannels better represent annular flow which is considered to exist at the limiting location.

1. Seed Model

This HOTROD three-dimensional model (Figure 19) represents a 1/6 section of a seed assembly in the core. The seed model was used to thermally analyze the hottest sector within the Type I module, as well as less limiting sectors of the seed region for the Type I, Type II, and Type III modules. The model, which includes both the heated rod portions and the unheated flow annulus between the seed shell and blanket guide tube, is divided into 36 subchannels. A total of 103-1/6 seed rods are represented by thirty power source rods as shown in Figure 19. The limiting subchannel, No. 12, is surrounded by small subchannels.

Subchannels Nos. 29 through 31 contain the outer row of fuel rods which are bounded by the inner surface of the seed support shell. In the model, these subchannels are interconnected (assuming negligible hydraulic resistance) at all axial levels with the subchannels (Nos. 33 through 36) defining the unheated flow annulus. This treatment permits maximum redistribution of coolant from the heated rod region into the annulus, thereby reducing coolant available to the rods. The modeling of the flow annulus as an integral part of the fuel region within the module is the same as that employed in the XITE modeling. Since the actual communication of heated fluid with the annulus in fact is limited to the discrete axial levels corresponding to the flow holes (with finite hydraulic resistance) in the seed shell, this treatment has been shown to be calculationally conservative for predicting a thermal limit.

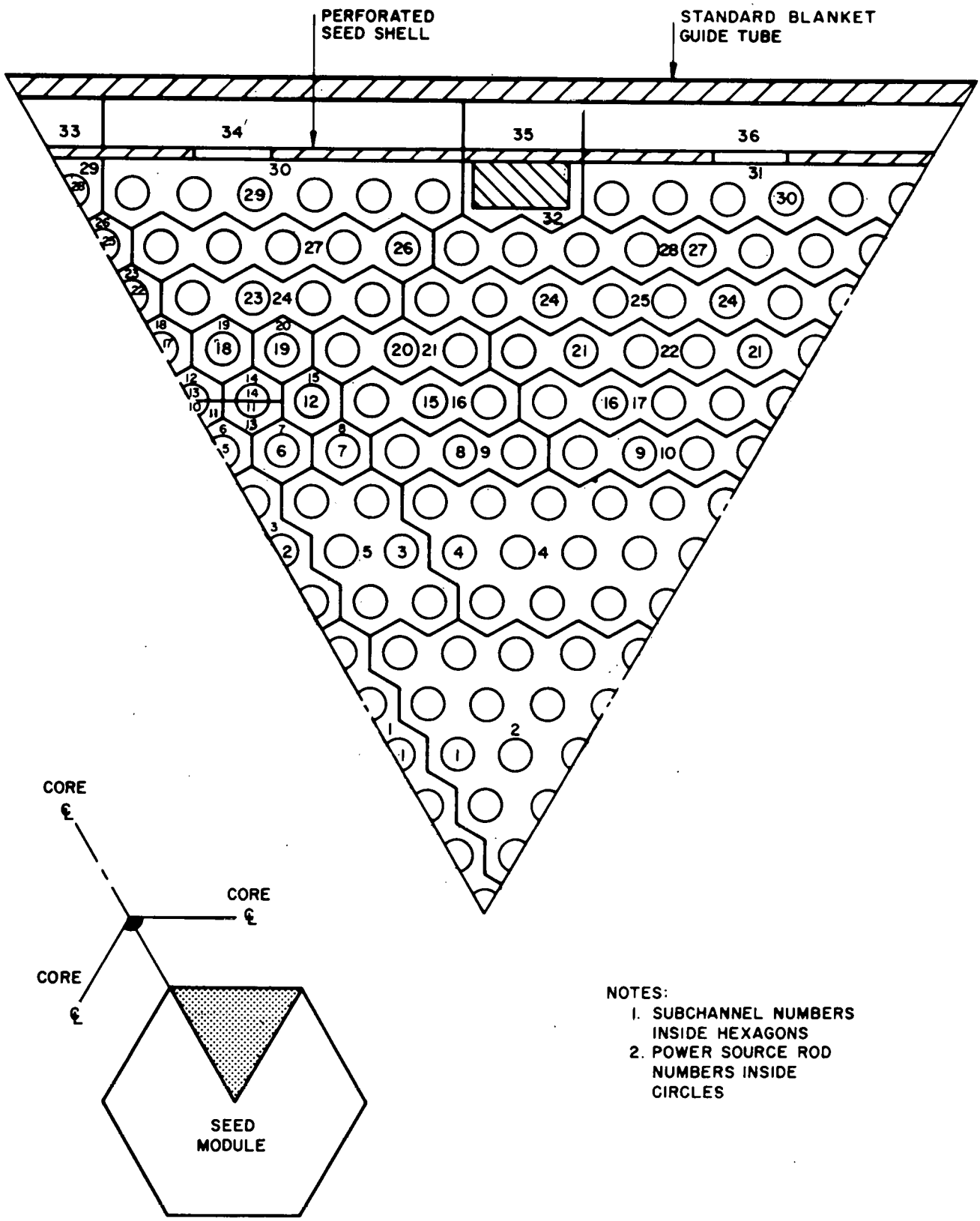


FIGURE 19. LWBR SEED HOTROD ANALYSIS MODEL

## 2. Blanket Model

The HOTROD three-dimensional blanket model, Figure 20, represents a blanket segment in the core (1/12 of the annular blanket region in a Type I module). This model consists of thirty-four subchannels with thirty-seven heated rods (and one-half of a structural post) represented by thirty power source rods. In contrast to XITE, the post is realistically represented with low heat output based on gamma heating. Subchannel No. 21 is thermally limiting and is surrounded by small subchannels having similar geometry. The portion of the blanket modeled is the hottest segment within the Type I module. The model was also applied to geometrically similar but thermally less limiting segments within the Types I, II and III modules, as shown in Figure 18.

## 3. Blanket and Power-Flattening-Blanket Interface Model

The model of the interface between the blanket and power-flattening blanket regions, as well as the boundary between the Type II and Type III modules, Figure 21, combines the coupled, but different, hydraulic characteristics and power distributions of these two fuel rod regions. (In the XITE treatment, the blanket and power-flattening blanket regions are separately modeled, as if hydraulically isolated). The interface model consists of forty subchannels, eighteen for the blanket and twenty-two for the power-flattening blanket regions. The fifty-two heated rods and two posts are represented by thirty power source rods. The hottest subchannels (Nos. 6, 14, 23 and 35) are assumed in the model to have no coolant mixing with the adjacent unheated and thus colder subchannel No. 28. Studies showed this treatment produces more conservative (lower) power predictions to reach thermal limits than had been noted when these hot subchannels were directly coupled to the colder subchannel No. 28.

## 4. Type IV Reflector Model

Figure 22 shows one-half of the symmetrical Type IV reflector region. This model consists of twenty-one subchannels which include one-hundred and fourteen reflector rods represented by twenty-one power source rods. The thermally limiting subchannels (Nos. 1, 2, 3, 4 and 7) are shown with more detail so that a transition in subchannel flow area toward the cooler zones is provided.

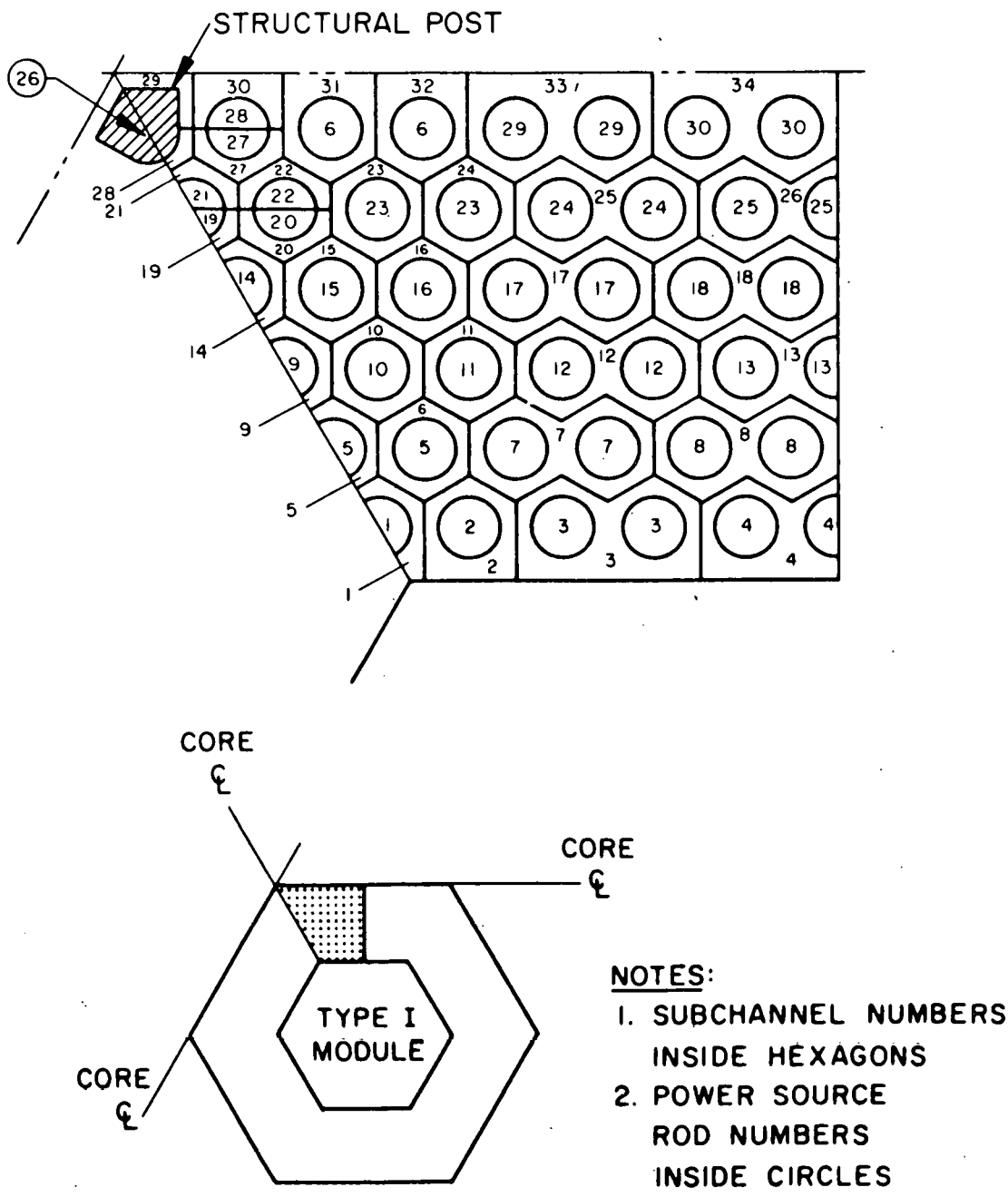


FIGURE 20. LBWR BLANKET HOTROD ANALYSIS MODEL

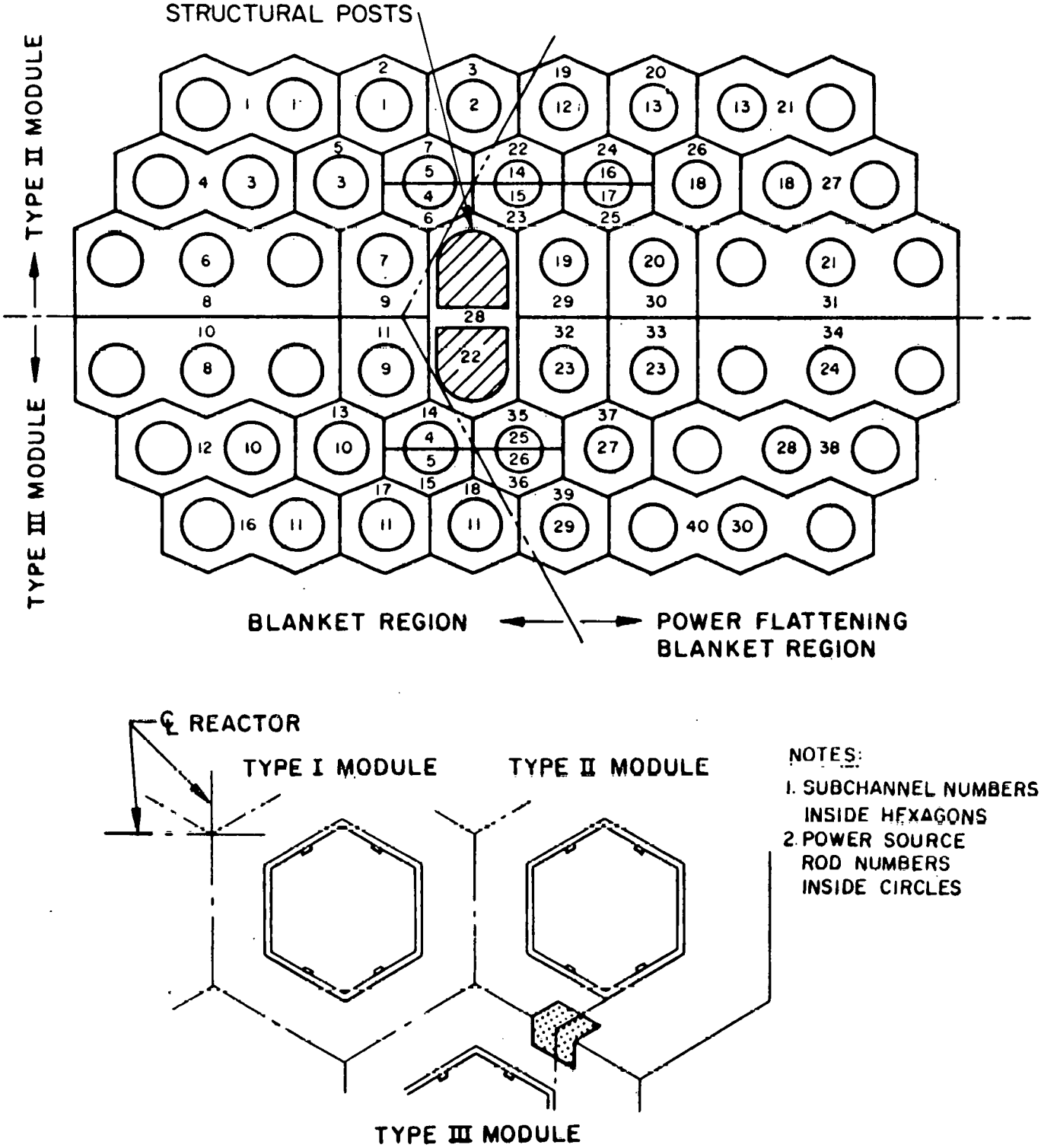


FIGURE 21. LWBR BLANKET/POWER-FLATTENING BLANKET HOTROD ANALYSIS MODEL

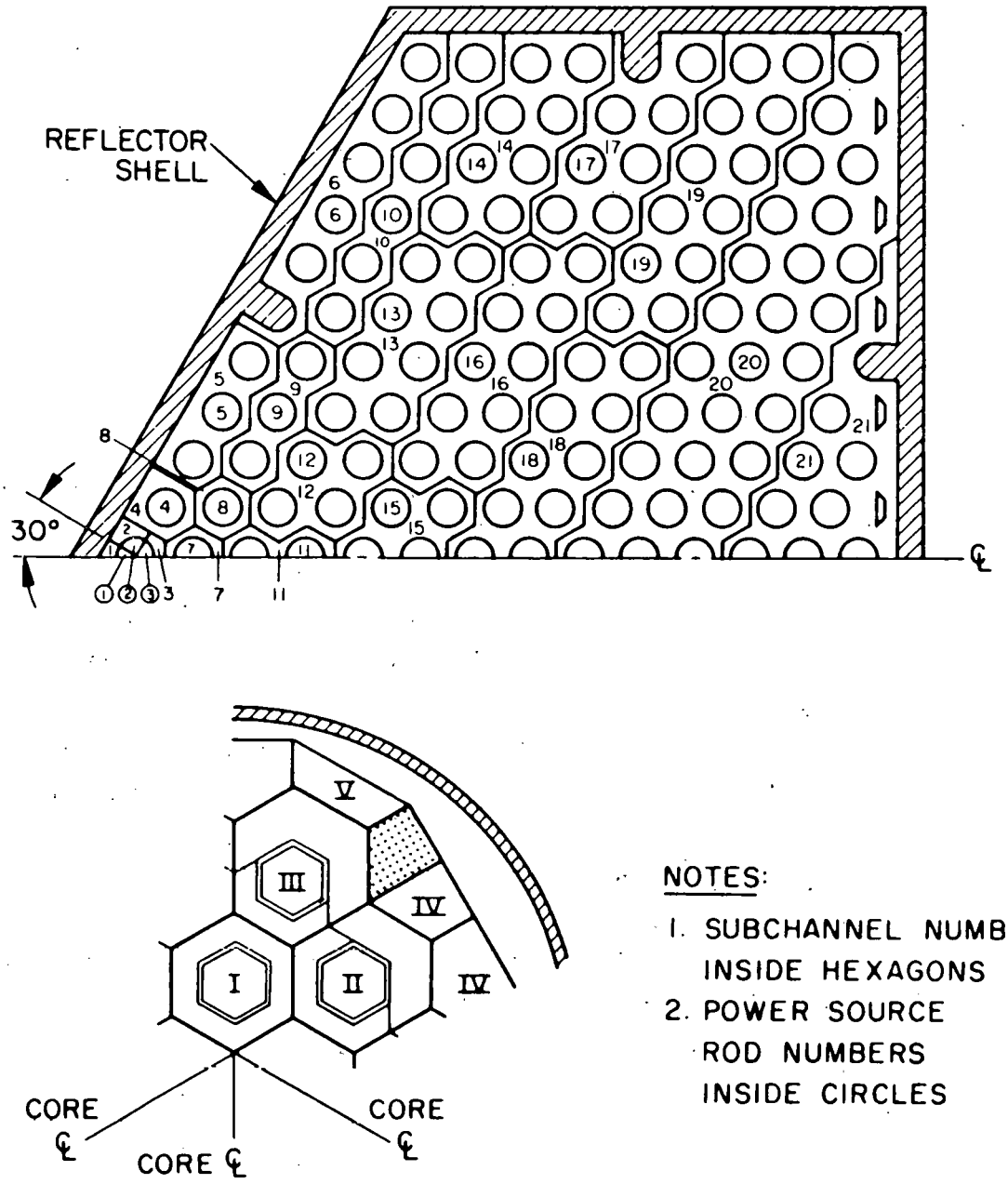


FIGURE 22. LWBR REFLECTOR HOTROD ANALYSIS MODEL

## VI. HOT CHANNEL ALLOWANCES

Off-nominal nuclear and mechanical conditions were accounted for in the thermal analysis by incorporating hot channel allowances. These include variations in local (hot subchannel) parameters which affect local flow and heat addition.

### A. Nuclear Allowances

Uncertainty factors for enthalpy rise and local heat flux appropriate to the nuclear model of the core, which model is described in Reference (22), accounted for potential variation between nominal-and worst-case power in the hot subchannels. These factors, shown in Table III-A and discussed in Reference (4), were incorporated into the XITE and HOTROD models to account for (a) the effect of movable-fuel-assembly misalignment which could cause power asymmetry and (b) differences between nuclear analytical calculations and nuclear mockup experiments. Table III-B presents factors which account for off-equilibrium poison conditions due to power changes, such as swingload operation and shutdowns, which affect core power distribution.

### B. Engineering (Mechanical) Allowances

The engineering factors account for variations in manufacturing tolerances, variations in fuel rod attributes, and possible biases in flow distribution. These factors are described in two categories below.

TABLE III

A. Nuclear Uncertainty Factors

Seed Region

| | Local Heat Flux Fuel Rod Rows | | | Rod Power (Enthalpy) All Rod Rows |
|---|---|---|---|---|
| | 1-12 | 13 | 14-15 | |
| Experiment/Calculation | 1.128 | 1.180 | 1.102 | 1.072 |
| Steady-state overpower* | 1.084 | 1.084 | 1.084 | 1.080 |
| Total Factor | 1.223 | 1.279 | 1.195 | 1.158 |

Blanket Region

| | Local Heat Flux Fuel Rod Rows | | | | Rod Power (Enthalpy) Fuel Rod Rows | | |
|---|---|---|---|---|---|---|---|
| | 1-2 | 3 | 4 | 5-6 | 1-3 | 4 | 5-6 |
| Experiment/Calculation | 1.207 | 1.176 | 1.166 | 1.187 | 1.098 | 1.120 | 1.140 |
| Steady-state overpower* | 1.071 | 1.071 | 1.071 | 1.071 | 1.076 | 1.076 | 1.076 |
| Total Factor | 1.293 | 1.259 | 1.249 | 1.271 | 1.181 | 1.205 | 1.227 |

*Includes module misalignment, calorimetric instrument accuracy, and generator load control variation.

TABLE III (cont'd)

Power-Flattening Blanket Region

| | Local Heat Flux Fuel Rod Rows | | | Rod Power (Enthalpy) All Rod Rows |
|---|---|---|---|---|
| | 1-2 | 3 | 4-10 | |
| Experiment/Calculation | 1.235 | 1.193 | 1.160 | 1.114 |
| Steady-state overpower* | 1.071 | 1.071 | 1.071 | 1.076 |
| Total Factor | 1.323 | 1.278 | 1.242 | 1.199 |

Reflector Blanket Region

| | Local Heat Flux | Rod Power (Enthalpy) |
|---|---|---|
| Experiment/Calculation | 1.187 | 1.140 |
| Steady-state overpower* | 1.071 | 1.076 |
| Total Factor | 1.271** | 1.227** |

* Includes module misalignment, calorimetric instrument accuracy and generator load control variation.

** Time dependent gamma heating factors were applied in addition to these factors. The variation in gamma heating factors for rod row 1 is 3.80 to 1.01 and for other rod rows is 2.20 to 1.00.

TABLE III (cont'd)

B. Thermal Off-Equilibrium Factors
(Relative to Equilibrium Poison Power Distribution)

| Core Lifetime, Hours | Seed Region | | Blanket Region ≠ | |
|---|---|---|---|---|
| | Local Heat Flux | Rod Power (Enthalpy) | Local Heat Flux | Rod Power (Enthalpy) |
| 0* | 1.0 | 1.0 | 1.0 | 1.0 |
| 100* | 1.0 | 1.0 | 1.0 | 1.0 |
| 1,000 | 1.015 | 1.015 | 1.008 | 1.008 |
| 3,000 | 1.048 | 1.048 | 1.028 | 1.028 |
| 5,000 | 1.038 | 1.038 | 1.036 | 1.036 |
| 10,000 | 1.018 | 1.018 | 1.050 | 1.050 |
| 14,500 | 1.038 | 1.038 | 1.050 | 1.050 |
| 18,000 | 1.055 | 1.055 | 1.050 | 1.050 |

* Core is off-equilibrium at 0 and 100 hours.

≠ Also applies to power-flattening blanket and reflector.

1. Heat Input Hot Channel Factors

Allowances for variations from nominal fuel loading and for heat-flux eccentricity were defined to account for tolerances on hot-channel heat input. Measured manufacturing data on fissile content of the fuel pellets were examined and used to establish a set of conservative fuel loading factors for local and rod-average heat fluxes. These factors are shown in Table IV.

Heat-flux eccentricity effects were also evaluated for their impact on enthalpy rise and local heat flux. Allowance was made for potential increased hot-channel enthalpy rise for a fuel pellet stack that could be eccentrically located inside a fuel rod and for oval cladding. Local heat-flux spikes due to any local pellet eccentricity within the cladding, nonuniform distribution of fuel porosity within the pellets, cladding ovality, and axial pellet gaps were also considered. Based on heat-flux-spike CHF tests, performed at Bettis (Reference (23)) and elsewhere (Reference (24)), these items were determined to have no effect on CHF.

2. Channel Flow Hot Channel Factors

Manufacturing tolerances, fuel-rod mechanical characteristics, and pressure maldistributions at the fuel-region inlet and outlet could influence the flow in the hot channel. These effects were covered by the use of hot-channel factors for rod bowing, rod pitch, and flow maldistribution. The corresponding factors are given in Table IV and are described below.

TABLE IV

HOT CHANNEL FACTORS

| | Rod Power (Enthalpy) Factor | | | | Local Heat Flux Factor | | | |
|---|---|---|---|---|---|---|---|---|
| | | | Power-Flattening | | | | Power-Flattening | |
| | Seed | Blanket | Blanket | Reflector | Seed | Blanket | Blanket | Reflector |
| 1. Fuel Loading (all lifetimes) | 1.008 | 1.004 | 1.004 | 1.010 | 1.013 | 1.009 | 1.009 | 1.019 |
| 2. Fuel Pellet Eccentricity (all lifetimes) | 1.012 | 1.005 | 1.005 | 1.02 | 1.000 | 1.000 | 1.000 | 1.000 |
| 3. Rod Bowing (linear between lifetimes shown) | | | | | | | | |
| 0 Hours | 1.022 | 1.05 (at 0 Hrs) 1.07 (>0 Hrs) | 1.07 | 1.07 | 1.022 | 1.05 (at 0 Hrs) 1.07 (>0 Hrs) | 1.07 | 1.07 |
| 100 Hours | 1.022 | 1.07 | 1.07 | 1.07 | 1.022 | 1.07 | 1.07 | 1.07 |
| 1,000 Hours | 1.023 | 1.07 | 1.07 | 1.07 | 1.023 | 1.07 | 1.07 | 1.07 |
| 13,000 Hours | 1.029 | 1.07 | 1.07 | 1.07 | 1.029 | 1.07 | 1.07 | 1.07 |
| 14,500 Hours | 1.030 | 1.07 | 1.07 | 1.07 | 1.030 | 1.07 | 1.07 | 1.07 |
| 18,000 Hours | 1.039 | 1.07 | 1.07 | 1.07 | 1.039 | 1.07 | 1.07 | 1.07 |
| 4. Rod Pitch (linear between lifetimes shown) | | | | | | | | |
| 0 Hours | 1.052 | 1.125 | 1.125 | 1.158 | 1.012 | 1.103 | 1.103 | 1.135 |
| 3,000 Hours | 1.067 | 1.092 | 1.092 | 1.158 | 1.026 | 1.071 | 1.071 | 1.135 |
| 5,000 Hours | 1.078 | 1.104 | 1.104 | 1.158 | 1.037 | 1.082 | 1.082 | 1.135 |
| 10,000 Hours | 1.087 | 1.113 | 1.113 | 1.158 | 1.045 | 1.091 | 1.091 | 1.135 |
| 18,000 Hours | 1.099 | 1.113 | 1.113 | 1.158 | 1.057 | 1.191 | 1.091 | 1.135 |
| 5. Flow Redistribution* | | | | | | | | |
| a. Plenum factor | 1.035 | 1.04 | 1.04 | 1.07 | | | | |
| b. Preferential crudding | Varies from 1.0 to 1.05 depending on time in life. Same for all regions. | | | | | | | |

*Applied to reduce flow rather than power.

Hot channel factors for rod bowing were analytically developed, based on power penalties derived from explicit consideration of bowing between grids. In the analysis, three rods were permitted to bow to a proximity of .009, .011, and .017 inch in the seed, blanket, and reflector regions, respectively. These values are compatible with the objectives of the fuel-rod/grid-support design to maintain spacings that would preclude significant adverse CHF effects. The bowing hot channel factor was determined as a CHF power penalty and, therefore, was included on both enthalpy and heat flux.

The hot channel factor for rod pitch accounts for variations in the hot-channel flow area due to grid-cell pitch tolerances, rod diameter tolerances, fuel-rod-cladding diameter shrinkage, cladding ovality, cladding grooving (shrinkage into pellet tapers), and cladding wear. Reference (3) provides additional details on these conditions. All of these effects shift rod center lines relative to each other and, therefore, affect flow area. These effects were evaluated on a worst-case basis using an explicit thermal analysis model.

Allowances were also applied to the hot channel flow to account for potential non-uniformity in inlet-and-outlet reactor-vessel plenum pressure and variations in crud deposits. These allowances assumed that the flow was reduced along the entire length of the channel.

## VII. SUMMARY OF THERMAL PERFORMANCE

### A. Critical Heat Flux Performance

Thermal evaluation of the core has demonstrated that the minimum thermal margin to CHF occurs during postulated accidents. The accidents considered include over-steam demand, loss-of-coolant (underflow), inadvertent scram of an individual movable fuel assembly, continuous withdrawal of the bank of movable fuel assemblies, low pressure, and cold water accidents. Each of these accidents has been evaluated in detail (see Reference (13)).

Table V summarizes the core thermal performance in terms of the minimum power ratio for steady-state operation and worst-case transients. The

TABLE V

SUMMARY OF THE MINIMUM POWER RATIOS
FOR LWBR STEADY-STATE/TRANSIENT CONDITIONS

| | Condition | Minimum Power Ratio |
|---|---|---|
| 1. | Nominal steady state | >2.0 |
| 2. | Design steady state (109% of rated power) | 1.35 |
| 3. | Reactivity insertion transient (126% of rated power) | 1.17 |
| 4. | Loss of flow accident (109% of rated power) | 1.24 |
| 5. | Loss of pressure accident (at the low scram setpoint and 109% of rated power) | 1.21 |
| 6. | Steam line rupture accident | 1.19 |

performance is based upon the as-built nuclear power description with the reactor at full flow. As noted in the table, the most thermally limiting accident is an overpower reactivity-insertion transient with a minimum DPR of 1.17.

Figure 23 shows the lifetime CHF power capability exceeds 100 percent of rated power for both the overpower and underflow accidents. The discontinuity in power capability at 2000 hours is a result of the assumed crud model. Figure 24 shows a balance between seed and blanket power capability has been achieved. A discussion of the core thermal response to the limiting overpower and underflow accidents follows.

1. Overpower Accident

The most limiting overpower accident is the power-range reactivity-insertion transient (RIT). The RIT results from continuous upward motion of the movable fuel bank (i.e., all twelve seed assemblies move upward simultaneously, resulting in a ramp-type power increase). An RIT involving outward motion of less than twelve movable fuel assemblies is prevented by interlocks. The maximum power reached in the hottest region of the core for the CHF-limiting RIT transient is equivalent to 126 percent of the steady-state core power. The accident is terminated by either the reactor operator, the high power-to-flow insertion setpoint, the high power-to-flow scram setpoint, or the high-coolant-temperature ($T_h$) scram setpoint. Since the movable-fuel-assembly bank RIT is a relatively slow transient, the thermal evaluations have been based on a conservative steady-state analysis with the core at 126 percent of rated power.

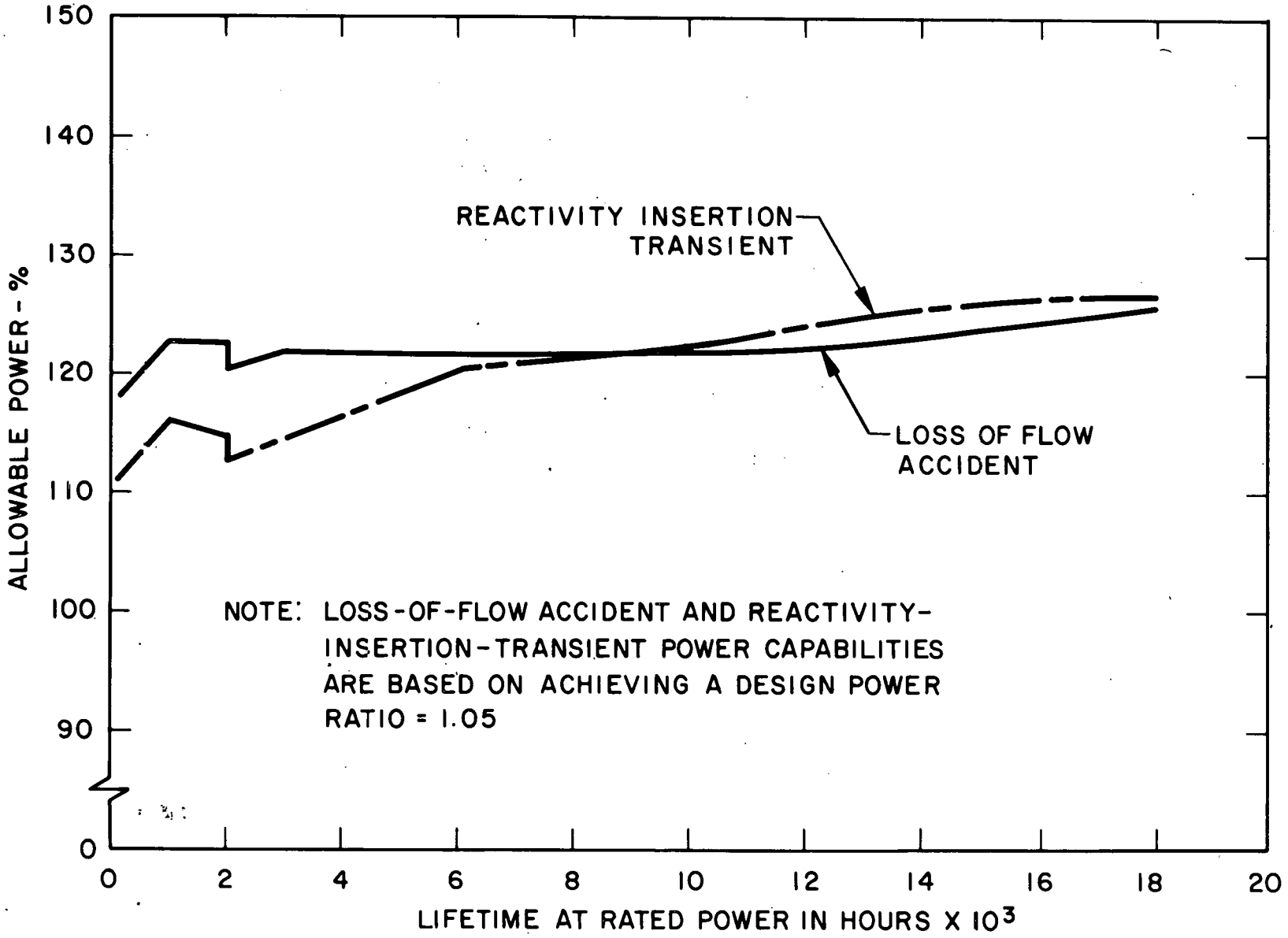


FIGURE 23. LWBR THERMAL CAPABILITY VS LIFETIME

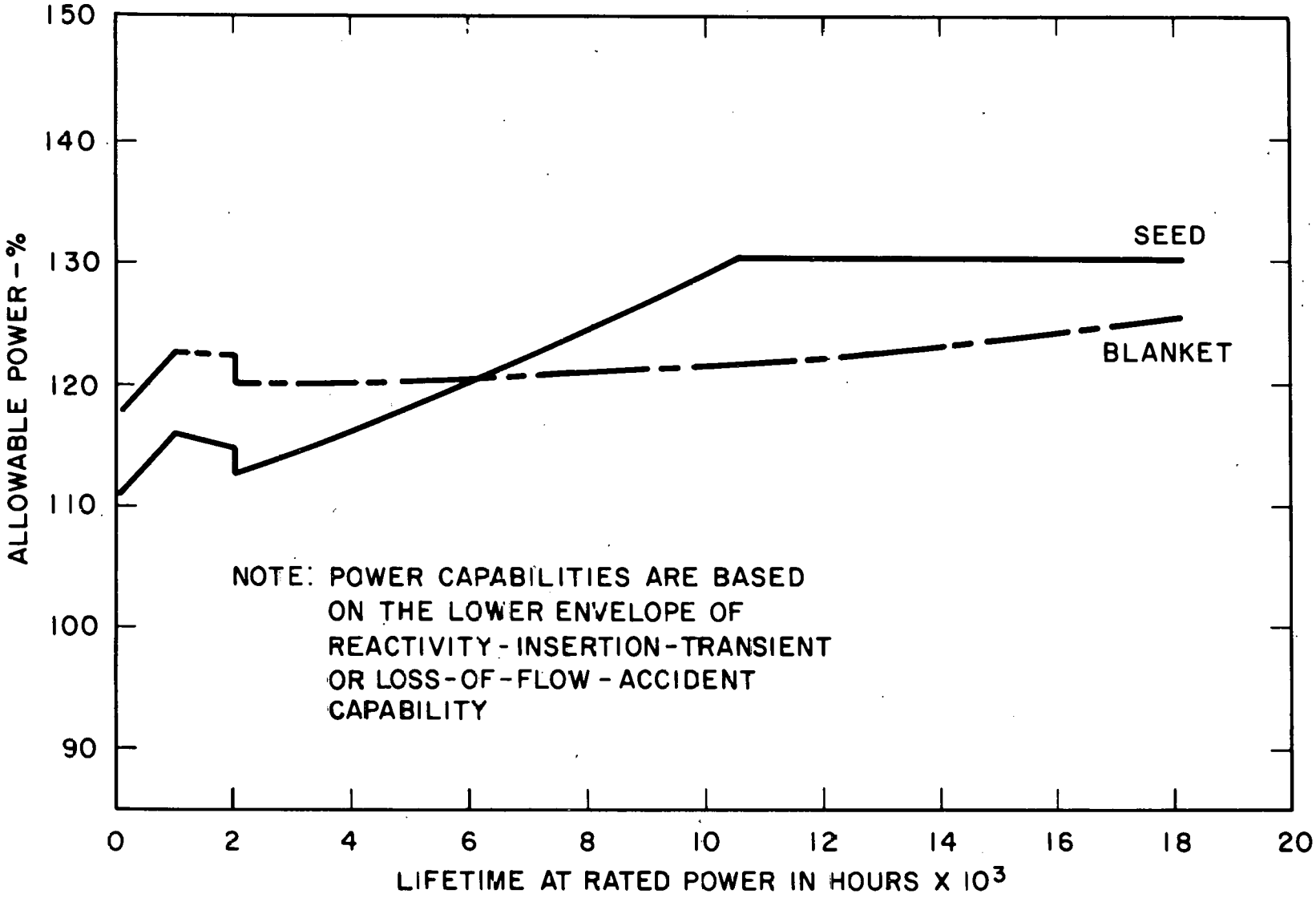


FIGURE 24. LWBR CHF POWER CAPABILITY (BY REGION) VS LIFETIME

The most thermally limiting seed-and-blanket hot channels are located in the Type I modules. The Type II and Type III seed and blanket fuel regions, the power-flattening blanket, and all reflector modules have a greater thermal margin than the Type I modules which have a minimum DPR of 1.17 (equivalent to 111-percent power capability) occurring at 100 hours. At 100 hours, the minimum DPR values for the Type II and Type III modules and the power-flattening blanket region are 1.22, 1.37, and 1.47, respectively, and their thermal margin increases thereafter throughout life. The core thermal margin increases early in life with the upward motion of the movable fuel bank, which results in a more favorable power distribution. The Type I seed is the thermally limiting core region until approximately 6000 hours after which the Type I blanket region becomes limiting.

The reflector modules have an inherently different lifetime thermal behavior than other module types. Since the reflector assemblies initially contain only thoria, the beginning-of-life heat flux is low. With increasing lifetime, the reflector thorium is transmuted to uranium-233 and the power generated in the reflector rods increases. The reflector performance capability decreases because of this increased power production. The minimum thermal margin in the reflector modules occurs at the end-of-life and is always greater than the most thermally limiting region of the core.

### 2. Loss-of-Flow Accident

A loss-of-flow accident is postulated to occur through (a) a loss of electrical power to one or more reactor coolant pumps, (b) a mechanical failure of a pump, such as a seized impeller, or (c) the inadvertent closure of a reactor coolant stop valve. A loss-of-flow causes a decrease in the reactor coolant flow rate with an attendant heatup of the coolant and a slowing down in the rate at which heat is removed from the fuel rods. To protect the core from reaching thermal limits, a reactor scram is initiated whenever the flow is less than the selected flow condition.

The thermal consequence of a loss-of-flow accident for the LWBR core has been significantly minimized through the use of flywheel generators (FWG). Each reactor coolant pump has an associated FWG which continues to provide electrical energy to the pump for some time after a loss of electrical pumping power. This energy input from the FWG reduces the rate of the coolant flow coastdown and thereby maintains a higher heat transfer rate from the fuel rods than would exist without the FWG's.

Figure 23 shows the lifetime variation of the CHF power capability for a complete loss-of-flow accident from an initial full flow condition. The Type I blanket region is limiting throughout core life for the complete loss-of-flow accident.

B. Flow Stability Performance

The flow stability analysis has been used to establish a lower bound on the power level required to induce an unstable flow condition in the hottest regions of the core. The power level to initiate flow instability has been found to exceed the maximum CHF power levels for the RIT and LOFA. The minimum design power ratio for flow instability is greater than 1.4 and occurs in the blanket region at beginning of life.

The seed flow-stability power limit at beginning of life is higher than that of the blanket even though the seed steady-state CHF limit is below that of the blanket. This condition arises because the axial flux distribution in the seed is skewed toward the top of the seed modules, whereas the blanket axial shape is flatter. Studies of flow instabilities, such as those reported in Reference (25), have shown that channels having flux shapes peaked toward the top are more stable than geometrically similar channels peaked otherwise. At end of life, the seed axial flux distribution shifts to the bottom of the module which thus causes this region to become more limiting than the blanket.

## VIII. QUALIFICATION

Thermal-analysis computer programs, models, and correlations used to evaluate the core performance were shown to be physically valid for thermal-hydraulic depiction of this core containing widely-ranging axial-and-radial heat-flux distributions, a closely spaced rod array, and a coupled-region interface. An extensive thermal/hydraulic test program provided the necessary confirmation. The thermal analysis programs with associated CHF and pressure-drop correlations were qualified using data from 19 rod bundles which provided over 850 CHF data points.

Initial scoping tests included rod bundles covering pitch-to-diameter ratios varying from 1.02 to 1.36, rod spacings from .015 to .090 inch, various axial-and-radial heat-flux distributions, and various grid designs. The tests were conducted at pressures ranging from 400 to 2000 psia, mass velocities from 0.1-to 4.0-million lbs/hr-ft$^2$, and inlet temperatures from 200°F to 600°F. Tests were also performed with prototypic bundles which incorporated the core fuel-region heat flux distributions, rod spacings, and the coupled interface region. The tests are summarized in Table VI and documented in Reference (26). The table identifies the test geometry, heat flux distributions, and the number of CHF data points obtained in each test.

The CHF and pressure-drop correlations used for core thermal evaluation were based on the data used to ensure the safe operation of the two previous Shippingport cores, PWR Core 1 and PWR Core 2. These correlations are described in Appendix A. A related design CHF correlation based on local fluid conditions was developed such that nearly all of the CHF data (including the rod bundle data described above) were conservatively predicted by the correlation. Figure 25 illustrates this result by showing the design-predicted CHF and the experimental CHF for rod bundle tests conducted in the core range of operation at 2000 psia and inlet temperatures from 500°F to

TABLE VI
ELECTRICALLY-HEATED ROD BUNDLE CHF TEST GEOMETRY

| | Test | Number of Rods | Rod Diameter (in.) | Pitch (in.) | Heated Length (in.) | Geometry Pitch/ Diameter | Infinite Array Hydraulic Diameter (in.) | Heat Flux Distribution Axial | Heat Flux Distribution Transverse | Support System** | Total Number of CHF Data Points |
|---|---|---|---|---|---|---|---|---|---|---|---|
| 1. | A.3.a | 20 | 0.75 | 0.765 | 94 | 1.02 | 0.1104 | Uniform | 1.5:1 | W | 60 |
| 2. | A.3.c.1 | 20 | 0.75 | 0.765 | 94 | 1.02 | 0.1104 | Uniform | 1.5:1 | W | 48 |
| 3. | A.3.c.2 | 20 | 0.75 | 0.765 | 94 | 1.02 | 0.1104 | Uniform | Uniform | W | 51 |
| 4. | A.4.a.1 | 20 | 0.25 | 0.340 | 54 | 1.36 | 0.2599 | Uniform | 1.5:1 | C | 71 |
| 5. | A.4.a.2 | 20 | 0.25 | 0.340 | 54 | 1.36 | 0.2599 | Uniform | 1.5:1 | C | 78 |
| 6. | A.4.b | 20 | 0.25 | 0.340 | 54 | 1.36 | 0.2599 | Uniform | Uniform | C | 75 |
| 7. | A.4.g | 20 | 0.250 | 0.340 | 54 | 1.36 | 0.2599 | Non-uniform | Uniform | C | 32 |
| 8. | A.6.a | 20 | 0.250 | 0.310 | 54 | 1.24 | 0.1738 | Uniform | 1.13:1 | C | 63 |
| 9. | A.4.d | 20 | 0.250 | 0.340 | 54 | 1.36 | 0.2599 | Uniform | Non-uniform | 66G | 50 |
| 10. | A.10.a | 20 | 0.250 | 0.340 | 54 | 1.36 | 0.2599 | Uniform | Non-uniform | 66G | 55 |
| 11. | A.4.e | 20 | 0.250 | 0.340 | 54 | 1.36 | 0.2599 | Uniform | Uriform | 66G | 25 |
| 12. | A.4.f.1 | 20 | 0.250 | 0.340 | 54 | 1.36 | 0.2599 | Uniform | Uriform | 67G | 33 |
| 13. | A.11.a.2 | 20 | 0.250 | 0.340 | 54 | 1.36 | 0.2599 | Uniform | Uriform | 67G | 7 |
| 14. | A.4.h.1 | 20 | 0.280 | 0.340 | 54 | 1.21 | 0.1750 | Uniform | Uriform | 68G | 45 |
| 15. | A.4.h.2 | 20 | 0.280 | 0.340 | 54 | 1.21 | 0.1752 | Uniform | Uniform | 68G | 55 |
| 16. | A.7.b | 20 | 0.301 | 0.368 | 84 | 1.22 | 0.1951 | Non-uniform | Non-uniform | 68G | 6 |
| 17. | A.1 | 29 | 0.303 | 0.358 | 85 | 1.21 | 0.1898 | Non-uniform | Non-uniform | 68G | 42 |
| 18. | A.9.a | 20 | 0.695 | 0.755 | 94 | 1.101 | 0.2335 | Uniform | 1.37:1.0 | 68G | 68 |
| 19. | A.2.a | 24 | 0.526/0.571 | 0.631 | 84 | 1.105/1.20 | 0.304/0.198 | Non-uniform | Non-uniform | 68G | 7 |

** Rod support system: G=Pre-1966 Grids; W=Warts (raised metal dimples on rods); C=Spacer collars; 66G, 67G and 68G refer to rod grid support system designs evolved in 1966, 1967, and 1968 (prototype).

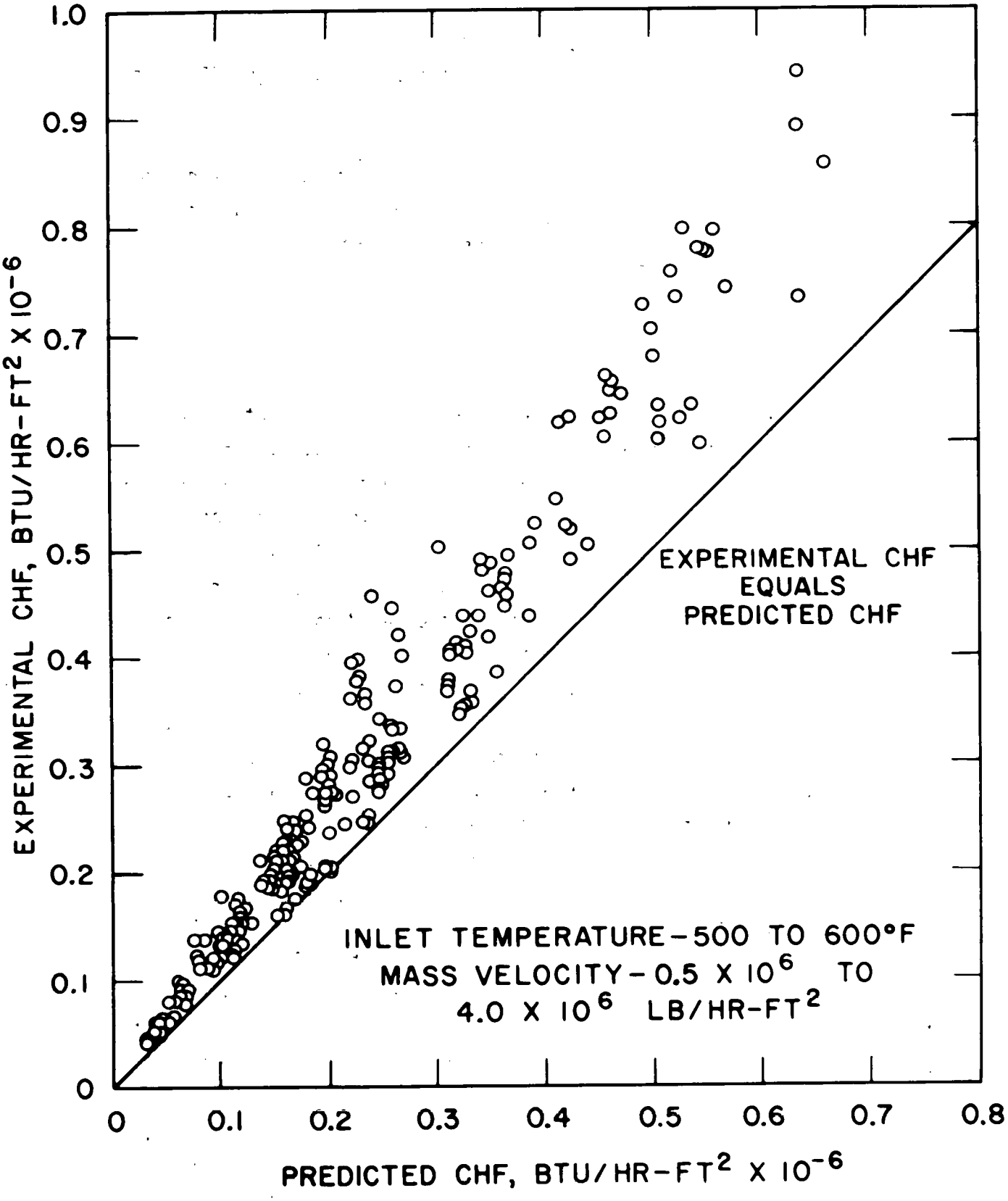


FIGURE 25. COMPARISON OF MEASURED AND PREDICTED CRITICAL HEAT FLUXES FOR LWBR TEST BUNDLES AT 2000 PSIA

600°F. All qualification predictions were performed using the HOTROD computer code.

Table VII summarizes the range of test conditions and the range of conditions over which the LWBR CHF and pressure-drop correlations were qualified. The range of LWBR core conditions is also shown in the table for comparison purposes.

## IX. CONCLUSION

The core for the Light Water Breeder Reactor was evaluated and shown to fulfill the objective of producing 236.6 thermal megawatts. Anticipated and potential modes of core operation, including steady-state behavior, normal transients, and postulated accidents were analyzed. The performance evaluation has shown that there is no CHF nor flow instability. The minimum design power ratios are 1.17 and 1.24 for the limiting overpower (reactivity-insertion transient evaluated at 26 percent above rated power) and underflow accidents (loss-of-flow accident involving all four coolant loops), respectively. In addition, a balance between seed and blanket power capability has been achieved. The evaluation accounted for special features of the core design which were devised to promote the breeding function. These features included tightly spaced three-dimensional rodded arrays comprising both hydraulically-coupled and -isolated core fuel regions.

The analytical procedure for evaluating core performance used fundamental reactor thermal principles such as the hot-and-nominal channel concept and nuclear/engineering allowances. The hot channels were defined using biases applied to power and flow and to instrument variation and uncertainty. Computer programs were used to integrate all components of the analytical procedure for performance evaluation. The programs combined the qualified procedures, core data, analytical models, and correlations for heat transfer and fluid flow with physical conservation laws. All procedures, models, allowances, and correlations were carefully qualified by analytical effort and an extensive program of heat-transfer and fluid-flow testing.

TABLE VII
LWBR CHF AND PRESSURE-DROP CORRELATION PARAMETER-RANGE SUMMARY

| | Parameter | Test Conditions | Qualification Conditions | Core Conditions |
|---|---|---|---|---|
| 1. | Pressure, psia | 400 to 2000 | 1200 to 2000 | 2200* |
| 2. | Mass velocity $lb/hr\text{-}ft^2 \times 10^6$ | 0.05 to 4.0 | 0.25 to 4.0 | 0.5 to 2.7 |
| 3. | Inlet temperature, °F | 200 to 500 | 400 to 600 | 480 to 530 |
| 4. | Heat flux | 0 to 98% of CHF for uniform radial, uniform radial, non-uniform axial and non-uniform radial and axial distributions | (Same as test conditions) | To 95% of CHF with non-uniform radial and axial heat flux-distribution |
| 5. | Hydraulic diameter, irches | 0.11 to 0.63 | (Same as test conditions) | 0.18 to 0.31 |
| 6. | Rod pitch-to-rod diameter ratio | 1.02 to 1.36 | (Same as test conditions) | 1.02 to 1.21 |
| 7. | Heated channel length, inches | 28 to 96 | (Same as test conditions) | 104** |
| 8. | Rod support structures | Warts, collars, and grids | (Same as test conditions) | Grids |

* Beginning-of-life nominal pressure is 2000 psia. Transient conditions can result in the pressure going to approximately 2200 psia.

** Core power is generated predominantly in the binary fuel region which is approximately 42 to 84 inches in length depending on rod type.

## X. REFERENCES


1. J.W. Stout, S. Lerner, K.D. McWilliams and J.R. Turner, Eds., "Summary of the Hydraulic Evaluation of LWBR", WAPD-TM-1386, Bettis Atomic Power Laboratory, Westinghouse Electric Corporation, April 1981.

2. D.R. Connors, S. Milani, J.A. Fest and R. Atherton, Eds., "Design of the Shippingport Light Water Breeder Reactor", WAPD-TM-1208, Bettis Atomic Power Laboratory, Westinghouse Electric Corporation, January 1979.

3. K.D. Richardson, "Summary of Fuel Rod Support System (Grids) Design for LWBR", WAPD-TM-1331, Bettis Atomic Power Laboratory, Westinghouse Electric Corporation, February 1979.

4. H.C. Hecker, "Summary of the Nuclear Design and Performance of the Light Water Breeder Reactor (LWBR)", WAPD-TM-1326, Bettis Atomic Power Laboratory, Westinghouse Electric Corporation, June 1979.

5. K.D. McWilliams and J.R. Turner, Eds., "Summary of Several Hydraulic Tests in Support of the Light Water Breeder Reactor Design", WAPD-TM-1253, Bettis Atomic Power Laboratory, Westinghouse Electric Corporation, May 1979.

6. P.R. Bengel, J.R. Turner and S.W. Sinderson, Jr., "Light Water Breeder Reactor Movable Fuel Hydraulic Balancing System", WAPD-TM-1143, Bettis Atomic Power Laboratory, Westinghouse Electric Corporation, July 1979.

7. "Technical Progress Report, Shippingport Atomic Power Station (PWR), for the Period January 26, 1978 to July 25, 1978", WAPD-MRP-150, Bettis Atomic Power Laboratory, Westinghouse Electric Corporation (1978), pp. 10-11.

8. L.H. Kemmet and J.A. Werling, Eds., "Shippingport Operations from Initial PWR Core 2 Power Operation to Power Operation After First Refueling", WAPD-332, Bettis Atomic Power Laboratory, Westinghouse Electric Corporation, June 1973.

9. R. T. Dressler, L.H. Kemmet and R.D. O'Hara, Eds., "Shippingport Operations During PWR Core 1 Depletion (December 1957 to February 1964)", WAPD-291, Bettis Atomic Power Laboratory, Westinghouse Electric Corporation, December 1968.

10. L.S. Tong, Boiling Heat Transfer and Two-Phase Flow, John Wiley and Sons, Inc., New York, 1965.

11. J.G. Collier, Convection Boiling and Condensation, McGraw-Hill Book Company (UK) Limited, London, 1972.

12. I. Veziroglu and S. Lee, "Boiling Flow Instabilities in a Cross-Connected Parallel-Channel Up-Flow System", ASME Paper No. 71-HT-12, 1971.

13. "Shippingport Atomic Power Station, Safety Analysis Report for the Light Water Breeder Reactor", Bettis Atomic Power Laboratory, Westinghouse Electric Corporation (1975).

14. R.P. Rose and R.S. Pyle, "XITE - A Digital Program for the Analysis of Two-Dimensional Boiling Flow Transients with Fluid Expansion", WAPD-TM-302, Bettis Atomic Power Laboratory, Westinghouse Electric Corporation, April 1963.

15. S.G. Beus, J.H. Anderson and R.J. DeCristofaro, "HOTROD - A Computer Program for Subchannel Analysis of Coolant Flow in Rod Bundles", WAPD-TM-1070, Bettis Atomic Power Laboratory, Westinghouse Electric Corporation, November 1973.

16. M. Legan in "New Programs from Argonne Computing Center," in "News from Correspondence", Nuclear News, 21, No. 4, 100-101 (March 1978).

17. I. Goldberg, L.L. Lynn and C.D. Sphar, "FIGRO - FORTRAN-IV Digital Computer Program for the Analysis of Fuel Swelling and Calculation of Temperature in Bulk-Oxide Cylindrical Fuel Elements", WAPD-TM-618, Bettis Atomic Power Laboratory, Westinghouse Electric Corporation, December 1966.

18. I. Goldberg, ibid., Addendum I, October 1967; Addendum II, April 1970.

19. I. Goldberg, "A Procedure for Calculation of Steady-State Temperature in Zircaloy-Clad, Bulk-Oxide Fuel Elements Using the FIGRO Computer Program", WAPD-TM-757, Bettis Atomic Power Laboratory, Westinghouse Electric Corporation, November 1969.

20. D.S. Rowe, "COBRA-II: A Digital Computer Program for Thermal Hydraulic Subchannel Analysis of Rod Bundle Nuclear Fuel Elements", BNWL-1229, Battelle North West Laboratory, February 1970.

21. S.G. Beus, "A Two-Phase Turbulent Mixing Model for Flow in Rod Bundles", WAPD-T-2438, Bettis Atomic Power Laboratory, Westinghouse Electric Corporation, November 1971.

22. L.B. Freeman, Ed., "The Calculational Model Used in the Analysis of Nuclear Performance of the Light Water Breeder Reactor (LWBR)", WAPD-TM-1314, Bettis Atomic Power Laboratory, Westinghouse Electric Corporation, August 1978.

23. E.P. Mortimore, S.G. Beus, "Critical Heat Flux Experiments with a Local Hot Patch in an Internally Heated Annulus", WAPD-TM-1419, Bettis Atomic Power Laboratory, Westinghouse Electric Corporation, February 1979.

24. V.N. Simolin, V.I. Eskov, et al., "Departure from Nucleate Boiling in channels with Heat Flux Peaking", Thermal Engineering, 17, No. 5, 95 (May 1970).

25. "Technical Progress Report for Pressurized Water Reactor (PWR) Project" WAPD-MEP-111, Bettis Atomic Power Laboratory, Westinghouse Electric Corporation, October 1964.

26. K.D. McWilliams, J.R. Turner, J.W. Stout and S. Lerner, "Unique Thermal and Hydraulic Features of the Light-Water Breeder Reactor", Transactions of the American Nuclear Society, 28, 575-576 (June 1978).

## XI. ACKNOWLEDGEMENT

The work required to develop and evaluate the thermal-hydraulic design of the LWBR core was performed by a large group of engineers over a period of several years. The management and technical guidance for this effort were provided by N.S. Sellers (deceased), R. Atherton, R.I. Miller, P.S. Marinkovich and J.R. Turner.

The authors are grateful to A.J. Stanko and M.R. Vaughan for their diligent typing effort and also to H.M. Dishong for her efforts in typing the final report.

APPENDIX A

ANALYTICAL CORRELATIONS

## A. Critical Heat Flux

The critical heat flux correlations used for LWBR thermal and hydraulic evaluation are similar to those previously used for the Shippingport Core, PWR Core 2 (References A-1, A-2, and A-3).

The following equations express the Shippingport critical heat flux correlation in terms of the coolant fluid conditions of local enthalpy, mass velocity, and pressure:

$$\frac{\phi_{CHF}}{10^6} = K\left[\frac{H^* - H_{CHF}}{H^* - H_o}\right]^{1/2}, \qquad \text{(Eq.A-1)}$$

where for best estimate calculations

$$K = 1 + \left[\frac{2000 - P}{800}\right]^2, \qquad \text{(Eq.A-2)}$$

$$H_o = 695 - 0.004(2000 - P)^{1.63}, \qquad \text{(Eq.A-3)}$$

$$H^* = H_q - [0.95]\ (H_{fg})\left(\frac{300}{H_{fg}}\right)^{10^6/G}, \qquad \text{(Eq.A-4)}$$

and for design calculations

$$K = 0.84\left[1 + \left(\frac{2000 - P}{800}\right)^2\right], \qquad \text{(Eq.A-5)}$$

$$H_o = 655 - 0.004(2000 - P)^{1.63}, \qquad \text{(Eq.A-6)}$$

and $$H^* = H_g - 0.275\ H_{fg} - 0.725\ \ (H_{fg})\ \left(\frac{300}{H_{fg}}\right)^{10^6/G}, \qquad \text{(Eq.A-7)}$$

with

$\emptyset_{CHF}$ = Critical Heat Flux, BTU/hr-ft$^2$.

G = Mass velocity, lb/hr-ft$^2$.

$H_{CHF}$ = Local enthalpy at the critical heat flux, BTU/lb.

$H_g$ = Enthalpy of saturated vapor, BTU/lb.

$H_{fg}$ = Latent heat of vaporization, BTU/lb.

P = Pressure, psia.

B. Heat Transfer

The Dittus-Boelter heat-transfer correlation has been confirmed in LWBR testing to be appropriate for core thermal and hydraulic evaluation. The correlation for conditions of fully developed turbulent flow in the absence of boiling is

$$h = \frac{CK_b}{D_e} (N_{RE})_b^{0.8} (N_{PR})_b^{0.4} \qquad \text{(Eq.A-8)}$$

The accuracy for reactor application is ± 20 percent with fully developed flow in the Reynolds Number range of $10^4$ to $10^6$ and bulk coolant temperatures of 100°F to 640°F. The accuracy is accounted for in the correlating coefficient C where:

h = heat transfer coefficient, BTU/hr-ft$^2$°F.

C = correlating coefficient with a value of 0.023 for the best estimate value, 0.019 for the lower limit, and 0.030 for the upper-limit heat-transfer coefficient.

$K_b$ = bulk water thermal conductivity, BTU/hr-ft°F, at the operating pressure.

$D_e$ = equivalent hydraulic diameter of the subchannel, ft.

$(N_{RE})_b$ = Reynolds Number evaluated at the bulk fluid temperature and the system operating pressure ($N_{RE} = DeG/\mu$).

$(N_{PR})_b$ = Prandtl Number evaluated at the bulk fluid temperature and the system operating pressure ($N_{PR} = C_p \mu / K_b$).

$\mu$ = fluid viscosity, lb/hr-ft.

$C_p$ = fluid specific heat, BTU/lb°F.

G = local mass velocity, lb/hr-ft$^2$.

In general, local nucleate boiling begins at a given location in a flow channel when the wall temperature ($T_w$) at that point reaches a certain level above the saturation temperature ($T_{sat}$) of the channel coolant. This difference is termed the wall superheat, $T_w - T_{sat}$. The Jens-and-Lottes correlation, Reference A-4, has been used to predict the wall superheat required for incipient local boiling:

$$(T_w - T_{sat}) = \frac{60 \left(\frac{\emptyset}{10^6}\right)^{1/4}}{\exp\left(\frac{P}{900}\right)} \quad , \qquad \text{(Eq.A-9)}$$

where

$T_w$ = wall temperature, °F.

$T_{sat}$ = saturation temperature, °F.

$\emptyset$ = local heat flux, BTU/hr-ft$^2$.

P = system pressure, psia.

This equation is used for those applications where the wall temperature itself is of primary concern. The term Jens-and-Lottes superheat is defined by $\Delta T_{J\&L} = (T_w - T_{sat})$ using the preceding equation. The transition from non-boiling to nucleate boiling is defined by the local hot-channel conditions which satisfy the following equation:

$$T_w = T_b + \emptyset / h \geq T_{sat} + \Delta T_{J\&L} \qquad \text{(Eq.A-10)}$$

where

$h$ = Dittus-Boelter forced-convection heat-transfer coefficient (lower limit for non-boiling wall temperature calculations), BTU/hr-ft$^2$-°F.

$T_b$ = bulk fluid temperature, °F.

$\emptyset$ = local surface heat flux, BTU/hr-ft$^2$.

$T_{sat}$ and $\Delta T_{J\&L}$ have previously been defined.

However, in determining the inception of boiling for channel vapor-fraction, pressure-drop and CHF-prediction purposes, the following modification is used:

$$T_w - T_b + \frac{\emptyset}{h} \geq T_{sat} \; . \qquad \text{(Eq.A-11)}$$

This is equivalent to setting the Jens-and-Lottes term to zero.

Equation (A-11) is used to provide a conservative bias in the calculation of the boiling lengths and point of boiling inception for vapor-fraction, pressure-drop, and CHF-prediction purposes since nucleate boiling is assumed to occur at the point where the wall temperature equals the saturation temperature.

The single-phase heat-transfer coefficient (h) in Equations (A-10 and A-11) is calculated from

$$h = \text{maximum of} \begin{cases} 0.023 \dfrac{K_L}{D_e} (N_{RE})_L^{0.8} (N_{PR})_L^{0.4} \\ 8.24 \dfrac{K_L}{D_e} \end{cases} , \qquad \text{(Eq.A-12)}$$

where the definitions are similar to those of Equation (A-8) except that the subscript L applies to the liquid. The lower expression of Equation (A-12) is the minimum value for the laminar-flow heat-transfer coefficient. In the single-phase region, the bulk and liquid properties are identical.

C. Pressure Drop

The pressure drop correlations used for LWBR analysis are as follows:

(1) Single phase entrance and exit pressure changes are given by

$$\Delta P_{ent} = \frac{G^2 v}{2g_c} (1 - \sigma^2 + K_c) \qquad \text{(Eq.A-13)}$$

and

$$\Delta P_{exit} = \frac{G^2 v}{2g_c} (\sigma^2 - 1 + K_e). \qquad \text{(Eq.A-14)}$$

(2) The elevation pressure drop is expressed as

$$\Delta P_c = \frac{g}{g_c} \int_{Z_1}^{Z_2} \bar{\rho}\,(Z)\, dz. \qquad \text{(Eq.A-15)}$$

(3) The acceleration pressure drop is expressed as

$$\Delta P_a = \frac{1}{g_c} \int_{Z_1}^{Z_2} \frac{1}{A}\, d\,(v^1 G^2 A). \qquad \text{(Eq.A-16)}$$

(4) The friction pressure drop between $Z_1$ and $Z_2$ is expressed as

$$\Delta P_f = \frac{1}{2g_c} \int_{Z_1}^{Z_2} n \frac{G^2}{D_e}\, dz, \text{ and} \qquad \text{(Eq.A-17)}$$

(5) The form loss across grids, base plates, and orifice plates is expressed as

$$\Delta P = K \frac{G^2 v}{2g_c}, \qquad \text{(Eq.A-18)}$$

where:

$\sigma$ = the ratio of the smaller to the larger flow area.

$G$ = mass velocity, $lb/hr\text{-}ft^2$, in the smaller area.

$K_c$ = unrecoverable contraction pressure loss coefficient.

$K_e$ = unrecoverable expansion pressure loss coefficient.

$g_c$ = gravitational constant, 32.2 $\frac{ft\text{-}lb_m}{lb_f\text{-}sec^2}$

$g$ = acceleration due to gravity, $\frac{ft}{sec^2}$

$\bar{\rho}$ = average density in a control volume bounded axially by $Z_1$ and $Z_2$.

$A$ = flow area, $ft^2$.

$Z$ = axial elevation, ft.

$v^1$ = specific volume, $ft^3/lb$.

$n = f_{iso}\ v\ F$.

$f_{iso}$ = friction factor (Reference A-5), dimensionless.

$v$ = average specific volume, $ft^3/lb$, in a control volume bounded axially by $Z_1$ and $Z_2$.

$F$ = a correlating parameter accounting for two-phase flow effects.

$K$ = Experimentally determined loss coefficient, dimensionless.

Qualification of the CHF and pressure-drop correlations is based on LWBR rod bundle tests (see main text). The heat-transfer correlations have been qualified using the LWBR tests and data from References A-4 and A-6.

## D. References


A-1. "Technical Progress Report for Pressurized Water Reactor (PWR) Project", WAPD-MRP-104, Bettis Atomic Power Laboratory, Westinghouse Electric Corporation, June 1963.

A-2. "Technical Progress Report for Pressurized Water Reactor (PWR) Project", WAPD-MRP-92, Bettis Atomic Power Laboratory, Westinghouse Electric Corporation, June 1961.

A-3. "Technical Progress Report for Pressurized Water Reactor (PWR) Project", WAPD-MRP-93, Bettis Atomic Power Laboratory, Westinghouse Electric Corporation, August 1961.

A-4. W.H. Jens and P.A. Lottes, "Analysis of Heat Transfer, Burnout, Pressure Drop, and Density Data for High Pressure Water", ANL-4627, Argonne National Laboratory, May 1951.

A-5. K.D. McWilliams and J.R. Turner, Eds., "Summary of Several Hydraulic Tests in Support of the Light Water Breeder Reactor Design", WAPD-TM-1253, Bettis Atomic Power Laboratory, Westinghouse Electric Corporation, May 1979.

A-6. J.G. Knudsen and D.L. Katz, Fluid Dynamics and Heat Transfer, McGraw-Hill Book Company, New York, 1958.

*U.S. GOVERNMENT PRINTING OFFICE: 1981/703-014/439